

FUNDAMENTAL ASPECTS OF ENGINEERING SCIENCE

EDITED BY:

Asts. Prof. Fatih UNAL

Lecturer Dr. Ahmet ERHAN AKAN

AUTHORS:

Prof. Fevzi KILICEL

Prof. Murat KISA

Asist. Prof. Mehmet HASKUL

Asist. Prof. Tulay GURSOY

Lecturer Dr. Hacer Sibel KARAPINAR



IKSAD

Publishing House

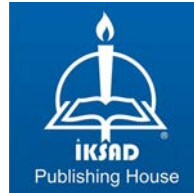
FUNDAMENTAL ASPECTS OF ENGINEERING SCIENCE

EDITED BY:

**Asts. Prof. Fatih UNAL
Lecturer Dr. Ahmet ERHAN AKAN**

AUTHORS:

**Prof. Fevzi KILICEL
Prof. Murat KISA
Asist. Prof. Mehmet HASKUL
Asist. Prof. Tulay GURSOY
Lecturer Dr. Hacer Sibel KARAPINAR**



Copyright © 2019 by iksad publishing house
All rights reserved. No part of this publication may be reproduced,
distributed, or transmitted in any form or by
any means, including photocopying, recording, or other electronic or
mechanical methods, without the prior written permission of the publisher,
except in the case of
brief quotations embodied in critical reviews and certain other
noncommercial uses permitted by copyright law. Institution Of Economic
Development And Social
Researches Publications®

(The Licence Number of Publicator: 2014/31220)

TURKEY TR: +90 342 606 06 75

USA: +1 631 685 0 853

E mail: iksadyayinevi@gmail.com

kongreiksad@gmail.com

www.iksad.net

www.iksad.org.tr

www.iksadkongre.org

It is responsibility of the author to abide by the publishing ethics rules.

Iksad Publications – 2019©

ISBN: 978-605-7695-24-6

Cover Design: İbrahim Kaya

August / 2019

Ankara / Turkey

Size = 16 x 24 cm

CONTENTS

EDITED BY

FUNDAMENTAL ASPECTS OF ENGINEERING SCIENCE

Asts. Prof. Fatih UNAL

Lecturer Dr. Ahmet ERHAN AKAN

1

CHAPTER 1

METAL ADSORPTION BEHAVIOR OF ACTIVATED CARBON PRODUCED FROM FRUIT WASTE: EFFECT OF COMPLEX TYPE AND AMOUNT OF ADSORBENT ON ADSORPTION

Lecturer Dr. Hacer Sibel KARAPINAR

Prof. Fevzi KILICEL

3 - 14

CHAPTER 2

ELASTIC BEHAVIOR OF THE CURVED BEAM ON THE PLANE STRAIN STATE CONDITION UNDER THE TEMPERATURE GRADING

Asist. Prof. Mehmet HASKUL

15 - 42

CHAPTER 3

FREE VIBRATION ANALYSIS OF A CRACKED BEAM WITH VARIABLE CROSS SECTION

Asist. Prof. Mehmet HASKUL

Prof. Murat KISA

43 - 68

CHAPTER 4

DETERMINATION OF AMOUNTS OF As, Cr, Pb and Mn ELEMENTS IN MOLASSES PRODUCED FROM CAROB: COMPARISON OF TRADITIONAL AND INDUSTRIAL PRODUCTION

**Lecturer Dr. Hacer Sibel KARAPINAR
Prof. Fevzi KILICEL**

69 - 78

CHAPTER 5

WA-XRD ANALYZES OF DIFFERENT KINDS OF COMPOSITE FILLING MATERIALS

Asist. Prof. Tülay GURSOY

79 - 101

FUNDAMENTAL ASPECTS OF ENGINEERING SCIENCE

Fundamental Aspects of Engineering Science presents a complete overview of the state of the fundamentals in engineering science. It is intended to meet the latest acknowledge requirements for engineers and brings together the essential material for a comprehensive understanding of engineering. The book is supported by engineering principles along with theory and formulas through examples and applications in each chapter. It covers international novel academic studies in engineering principles along with theory and formulas through examples and applications in each chapter developed by the authors who assume the previous background in engineering studies. Users will find a perfect blend of the interdisciplinary approach to fundamental aspects of engineering science.

Asts. Prof. Fatih UNAL
Lecturer Dr. Ahmet ERHAN AKAN

CHAPTER 1

METAL ADSORPTION BEHAVIOR OF ACTIVATED CARBON PRODUCED FROM FRUIT WASTE: EFFECT OF COMPLEX TYPE AND AMOUNT OF ADSORBENT ON ADSORPTION

Lecturer Dr. Hacer Sibel KARAPINAR¹

Prof. Fevzi KILIÇEL²

¹*Scientific and Technological Research & Application Center, Karamanoğlu Mehmetbey University, 70200, Karaman, Turkey, sibelkarapinar@kmu.edu.tr*

²*Department of Chemistry, Karamanoğlu Mehmetbey University, 70200, Karaman, Turkey, fevzi@kmu.edu.tr*

1. INTRODUCTION

Environmental pollution is a negligible problem that affects the health of people by increasing industrialization. For example, large quantities of contaminants are discharged to the environment without pretreatment (Alvarez et. al., 2018; Rozi et. al., 2018). These pollutants mainly include organic dyes, heavy metal ions, excess used antibiotics, various disruptive chemicals and the like. Adsorption is the most successful and promising approach due to its ease of use, low cost, no secondary contaminants and wide availability of adsorbent materials (San Miguel et. al., 2006; Crini, 2006). Carbon materials, especially the most commonly used material, have been used for a long time to remove heavy metals due to their high surface area, porosity and low cost (Islam et al., 2017). Adsorption processes with activated carbon are widely used in the separation of dangerous materials like heavy metals due to their high adsorption ability (Kamravaei et. al., 2017). From an economic and environmental point of view, re-use of activated carbon by regeneration is strongly required on industrial scales (Sun et. al., 2017). In the present study, the attempts have been made to remove metal ions from aqueous solution using activated carbon prepared from *eriobotrya japonica* seeds as a low-cost adsorbent. In addition, the amount of adsorbent and the effect of complex species were investigated. According to the results, it was determined that the adsorption capacity increased as the amount of activated carbons used in the adsorption increased. In addition, the metal holding capacities of the ligands were found to be good.

2. MATERIALS and METHODS

Materials: Eriobotrya Japonica (EJ) was used activated carbon preparation and was gathered from markets in Karaman.

Preparation of activated carbons: The EJ seeds were distracted from the fruit and desiccated by heating at 90 °C over night. After that, the raw material was milled in grinder and screened to 20-200 mesh particle dimension by standard sieves. The EJ powder was mixed with the phosphoric acid in rates 1/1 (20g/20g). 300 ml of distilled water was added to the mixture. The mixtures were dehydrated in an oven at 105 °C for about 36 h. Carbonization was carried out in a hollow cylindrical stainless steel reactor of 30 cm in width. The reactor has an inlet and a gas outlet. It is heated with a tubular oven with a temperature programmer. The samples were heated to final temperatures of 400, 500 °C with 5 °C min⁻¹ heating rate samples and they were stored for 3 hours at final temperatures. After cooling to room temperature, the resulting activated carbon was boiled in 2 M HCl to remove impurities. Then it was filtered and washed with pure water until the pH 7. It was dried at 110 °C in an oven for about 16 h and weighed to calculate the yield.

Adsorption studies: In the adsorption of chrome and nickel elements on activated carbon, glass columns with an inner diameter of 1.5 cm and length of 20 cm were used as experimental setup. 0.4, 0.6, 0.8 g of activated carbons produced at different temperatures were taken into columns. Then, 15 mL of the beaker was taken from the standard solution with Cu(II) (0.02 mg/L), Ni(II) (0.05 mg/L) ions and 4 mL of

benzenesulfonamide (B) and N,N'-ethylenebis (acrylamide) (N) ligands were added. Beaker solution was added to the column after 60 minutes. The prepared solution was kept on the column for 90 minutes and passed through the column. The column was measured in FAAS.

The adsorption capacity of Cr^{+3} and Ni^{+2} are given by the following formula:

$$q_e = (C_o - C_e) \times V / m$$

q_e = Adsorption capacity of adsorbent (mg/g, mol/g)

C_o = Initial concentration of adsorbate (mg/L, mol/L)

C_e = Concentration of adsorbate (adsorbed substance) at equilibrium (mg/L, mol/L)

V = Solution volume (L)

m = weight of adsorbent (g)

3. RESULTS

According to Fig. 1, 2; when the SEM images of each active carbon are taken, AC has a porous structure. The obtained AC displayed a highly porous structure with various sizes of mesopores and macropores. FT-IR spectra of AC-H₃PO₄ (400 and 500 °C), are given in Figure 3.

According to Figure 3, the existence of the wide and intensive absorption peak at 3600-2000 cm⁻¹ shows the O-H stretching oscillation of cellulose, hemicellulose, absorbed water, pectin and lignin. The asset of the peak at 1790 cm⁻¹ display the carbonyl (C=O) tension oscillation of the carboxyl classes of pectin, hemicellulose and lignin. The peaks in the range of 1250-1000 cm⁻¹ may belong to the C-O stretching oscillation of alcohols and carboxylic acids (Njoku et. al., 2013). The peaks at 1600 and 1400 cm⁻¹ are related to the C-O oscillations of the carboxyl groups on the acidic oxygen surface and play a major role in the adsorption of heavy metals.

Adsorption capacity of adsorbents Cu(II) and Ni(II) ions are given in Table 1. The linear Langmuir isotherm graph of Cu(II) and Ni(II) ions adsorbed on activated carbon is given in Fig. 4.

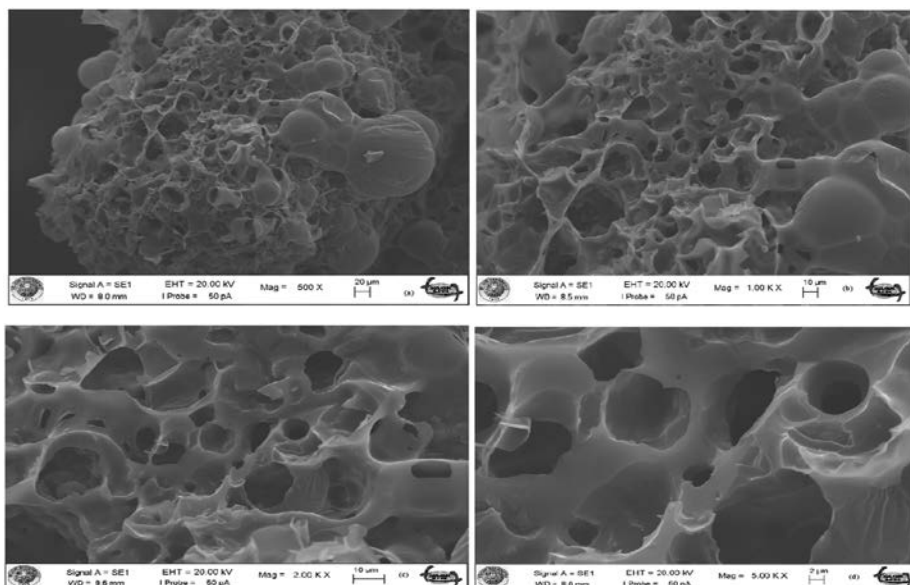


Figure 1. SEM images of activated carbon produced at 400 °C carbonization temperature (500 (a), 1000 (b), 2000 (c), 5000 (d)-fold magnification)

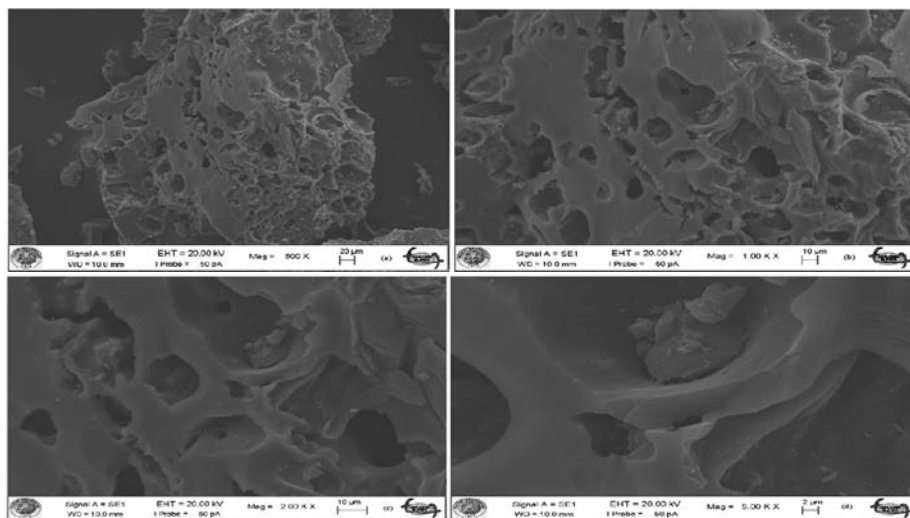


Figure 2. SEM images of activated carbon produced at 500 °C carbonization temperature (500 (a), 1000 (b), 2000 (c), 5000 (d)-fold magnification)

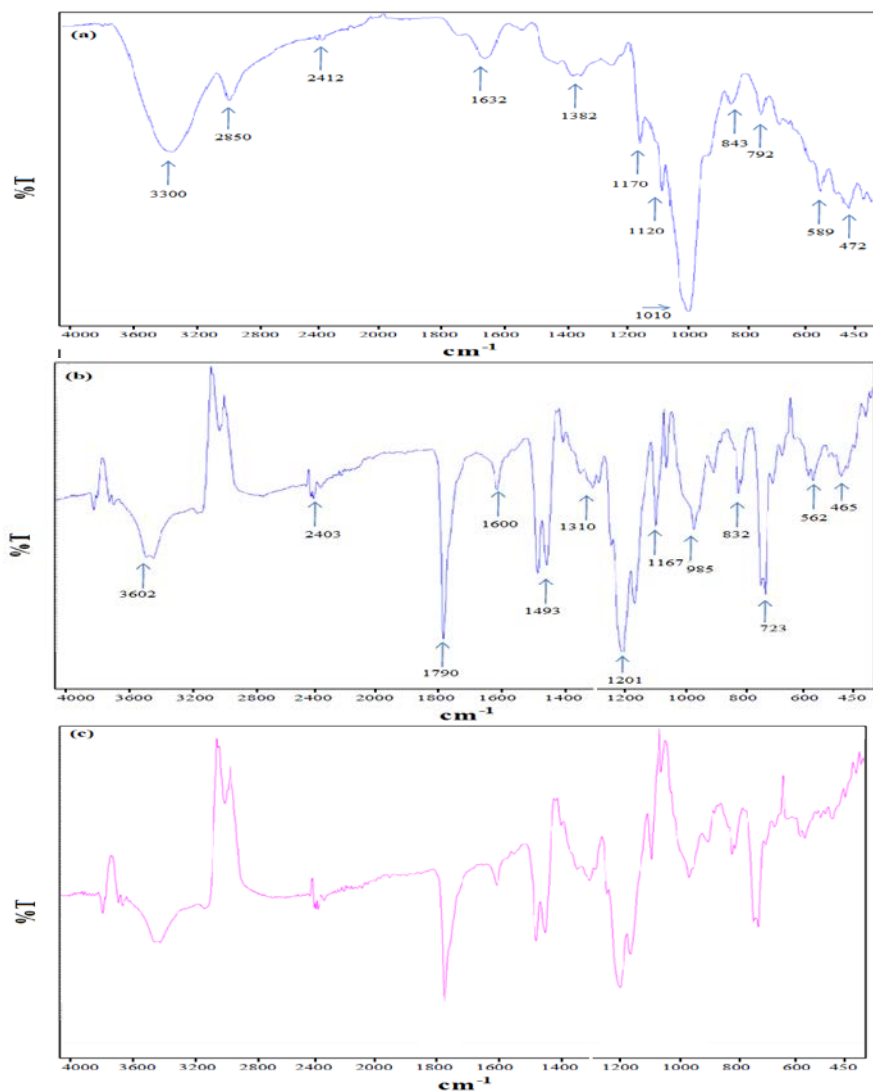


Figure 3. Activated carbon- H_3PO_4 FTIR spectra; (a) Raw material prior to carbonized impregnation with phosphoric acid, (b) AC- H_3PO_4 (400 °C), (c) AC- H_3PO_4 (500 °C)

Table 1. Adsorption capacity of adsorbents Cu(II) and Ni(II) ions

Activated carbon	%Ni(II)	%Cu(II)
AC-400 °C (B) (0.4 g adsorbent)	91.52	96.32
AC-400 °C (B) (0.6 g adsorbent)	93.69	97.91
AC-400 °C (B) (0.8 g adsorbent)	92.12	95.34
AC-500 °C (B) (0.4 g adsorbent)	95.31	97.56
AC-500 °C (B) (0.6 g adsorbent)	96.43	97.63
AC-500 °C (B) (0.8 g adsorbent)	96.21	97.91
AC-400 °C (E) (0.4 g adsorbent)	70.63	73.65
AC-400 °C (E) (0.6 g adsorbent)	71.15	73.98
AC-400 °C (E) (0.8 g adsorbent)	71.21	72.57
AC-500 °C (E) (0.4 g adsorbent)	72.38	73.02
AC-500 °C (E) (0.6 g adsorbent)	73.89	74.21
AC-500 °C (E) (0.8 g adsorbent)	70.32	73.16

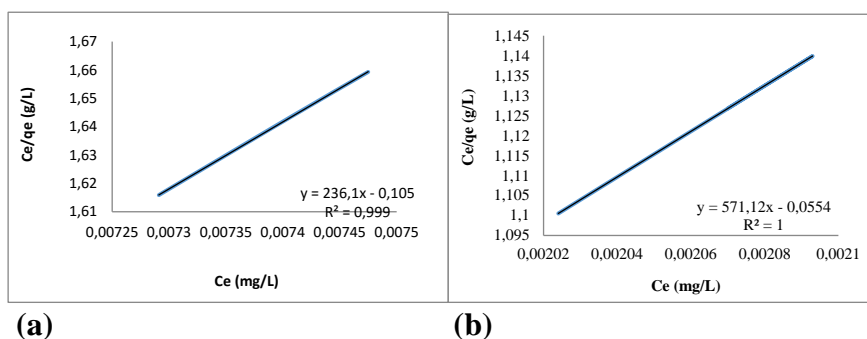


Figure 4. Linear Langmuir Isotherm of Ni(II) (a), Cu(II) (b) ions adsorbed on activated carbon

4. DISCUSSION

The results show that the chemical activation with H_3PO_4 from EJ seed is good in terms of specific surface field, pore improving and the structural order of activated carbon. EJAC- H_3PO_4 can be contemplated as an excellent low-cost and eco-friendly adsorbent. It was determined that activated carbons absorbed $\text{Cu}(\text{II})$ ions from water better than $\text{Ni}(\text{II})$ ions. In addition, it was determined that the adsorption capacity of activated carbons produced by increasing the activation temperature decreased. The metal holding capacity of the benzenesulfonamide ligand was found to be superior to the $\text{N,N}'$ -ethylenebis (acrylamide) ligand.

5. REFERENCES

- Alvarez, P. J., Chan, C. K., Elimelech, M., Halas, N. J., & Villagrán, D. (2018). Emerging opportunities for nanotechnology to enhance water security. *Nature nanotechnology*, *13*(8), 634.
- Crini, G. (2006). Non-conventional low-cost adsorbents for dye removal: a review. *Bioresource technology*, *97*(9), 1061-1085.
- Islam, M. A., Ahmed, M. J., Khanday, W. A., Asif, M., & Hameed, B. H. (2017). Mesoporous activated carbon prepared from NaOH activation of rattan (*Lacosperma secundiflorum*) hydrochar for methylene blue removal. *Ecotoxicology and environmental safety*, *138*, 279-285.
- Njoku, V. O., Foo, K. Y., & Hameed, B. H. (2013). Microwave-assisted preparation of pumpkin seed hull activated carbon and its application for the adsorptive removal of 2, 4-dichlorophenoxyacetic acid. *Chemical engineering journal*, *215*, 383-388.
- Kamravaei, S., Shariaty, P., Jahandar Lashaki, M., Atkinson, J. D., Hashisho, Z., Phillips, J. H., ... & Nichols, M. (2017). Effect of beaded activated carbon fluidization on adsorption of volatile organic compounds. *Industrial & Engineering Chemistry Research*, *56*(5), 1297-1305.
- Rozi, S. K. M., Shahabuddin, S., Manan, N. S. A., Mohamad, S., Kamal, S. A. A., & Rahman, S. A. (2018). Palm fatty acid functionalized Fe₃O₄ nanoparticles as highly selective oil

adsorption material. *Journal of nanoscience and nanotechnology*, 18(5), 3248-3256.

San Miguel, G., Lambert, S. D., & Graham, N. J. (2006). A practical review of the performance of organic and inorganic adsorbents for the treatment of contaminated waters. *Journal of Chemical Technology & Biotechnology: International Research in Process, Environmental & Clean Technology*, 81(10), 1685-1696.

Sun, Y., Zhang, B., Zheng, T., & Wang, P. (2017). Regeneration of activated carbon saturated with chloramphenicol by microwave and ultraviolet irradiation. *Chemical Engineering Journal*, 320, 264-270.

CHAPTER 2

**ELASTIC BEHAVIOR OF THE CURVED BEAM ON
THE PLANE STRAIN STATE CONDITION UNDER
THE TEMPERATURE GRADING**

Assist. Prof. Mehmet HASKUL¹

¹ Sirnak University, Department of Engineering, Mechanical Engineering, Sirnak, Turkey, mehmethaskul@sirnak.edu.tr

INTRODUCTION

In this study, the elastic behavior of the cylindrically curved beam, which is functionally graded for temperature grading in radial direction, has been analytically investigated. The temperature distribution varies steadily state as a function of the radial coordinate. The beam is assumed to be in the plane strain state. In addition, the beam is fixed in the cylindrical direction by rigid supports and these supports allow displacement on the ends surfaces of the beam, but the radius of curvature of the central surface of the beam remains constant. When the temperature is applied in the radial direction to the curved beam, the bending moment occurs at both ends due to the support of the supports and the beam is forced to operate under both thermal and mechanical loads. The elasticity modulus of the functionally graded beam is assumed to vary with the power law in relation to the thickness of the beam. In addition, the effect of the vary in the power law parameter and with the general mixture law, all material properties of the beam (modulus of elasticity, density, thermal expansion coefficient, thermal conductivity coefficient and uniaxial yield stress) except for Poisson's ratio change in radial direction. Thus, all material properties of the beam vary depending on the power law. Elastic behavior of the curved beam positive and negative temperatures were examined. Elastic state is considered according to von Mises yield criterion. The numerical results were obtained for steel/aluminum curved FGM beam.

Functionally graded material (FGM) are a composite material consisting of a gradient from one surface to another. In characteristics,

this compositional diversity improves the thermal and mechanical behavior of the system. In a structure made of FGM, elasticity, density, heat conduction, etc. have various production methods to meet different needs. The use of the functionally graded materials has been increasing and these composite materials have attracted scientific attention e.g. widely-used thermal assembly process, the studies (Noda, 1999; Zimmerman and Lutz, 1999; Shao, 2005; Awaji and Sivakumar, 2001; Evci and Gulgec, 2018; Arslan and Mack, 2015; Peng and Li, 2010;), modeling, fabrication and properties of the functionally graded materials (Naebe and Shirvanimoghaddam, 2016; Nemat-Alla et al., 2011; Birman and Byrd, 2007; Sobczak and Drenchev, 2013).

Deformation behavior of curved beams and methods to increase the material limits of such bars under varying loads have received significant attention by researchers. Elastic analysis of wide curved bar have been given by Timoshenko and Goodier (1970). Shaffer and House (1957, 1954) have been obtained equations for the elastic-plastic stress distribution a perfectly plastic wide curved bar and displacements a perfectly plastic incompressible material wide curved bar subjected to pure bending. Arslan and Mack (2014) presented analytical solutions for the elastic-plastic behavior of the panel under the thermal load. Analytical solution of linear hardening elastic-plastic material in the work are investigated (Dadras, 2001; Eraslan and Arslan, 2008) and obtained the behavior for nonlinear hardening material by Arslan and Eraslan (2010). The classical shell theory have studied the nonlinear behavior of curved panels under pressure and temperature (Librescu et

al., 2000; Duc and Van Tung, 2010). Kiani and et al. (2012) investigated the dynamic behavior of the functionally graded panel in the radial direction subjected to thermal and mechanical loads. Dryden (2007) studied elastic bending stresses of functionally graded curved bars. Mohammadi and Dryden (2008) investigated the the thermoelastic stress field in a functionally graded curved beam. Their work is obtained analytically where the radial variation of the stiffness is represented by a fairly general form. Eraslan and Akis (2006) have analytical solutions for plane stress and plane strain for the functionally graded rotating shaft and solid disk.

In this study, analytical solutions for the stress analysis in cylindrically curved beam are derived under assumption of plane strain state. The analytical solution for the elastic limit and displacements of the FGM curved beam subjected to thermal and mechanical loads is obtained. It is assumed that the material properties of the beam (modulus of elasticity, density, coefficient of thermal expansion, coefficient of thermal conduction and yield stress) are varied in radial direction depending on the power law.

MATHEMATICAL MODEL

Elastic behavior cylindrically FGM curved beam with a rectangular cross section (see Fig. 1) under plane strain state condition is investigated. Figure 1 shows the geometry of the curved beam with the inner radius a and the outer radius b .

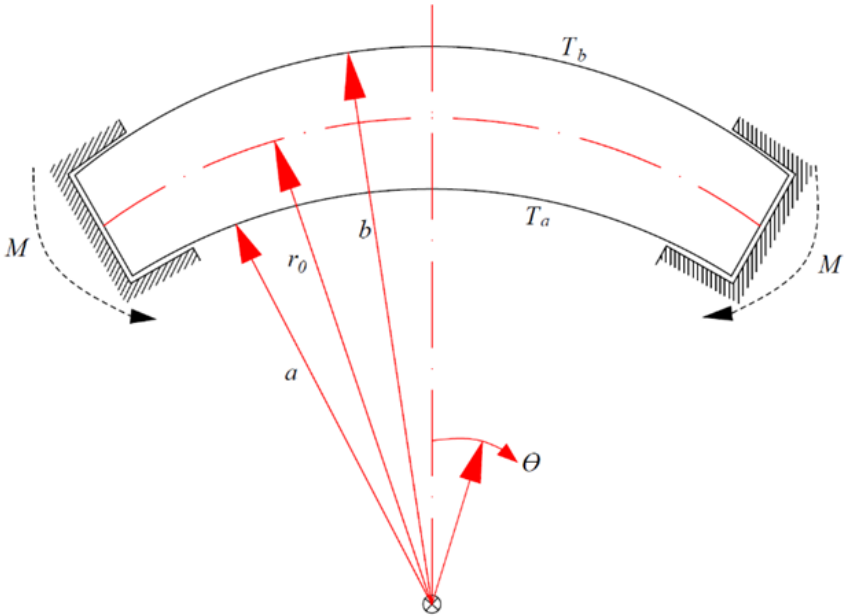


Figure 1. Coordinate system used and curved beam

Statement of the Problem

The subject of the current investigation is a curved beam (see Fig.1) with stress-free inner and outer cylindrical surfaces,

$$\sigma_r \Big|_{r=a} = 0, \quad (1)$$

$$\sigma_r \Big|_{r=b} = 0. \quad (2)$$

In the radial direction, the curved FGM beam is in plane strain state ($\varepsilon_z=0$) and is radially displaced by varying $T=T(r)$ temperature distribution. Displacement of the beam in the radial direction;

$$r = r_0 : \quad u = 0 \quad (3)$$

Since it is assumed that the initial middle surface where $r_0 = (a + b)/2$ does not undergo a radial displacement. Moreover, the couple moments M that occur at the rigid supports at the circumferential direction can be defined as

$$M = \int_a^b \sigma_\theta r dr \quad (4)$$

Basic Equations

The strain-displacement relations;

$$\varepsilon_r = \frac{du}{dr}, \quad (5)$$

$$\varepsilon_\theta = \frac{u}{r} + \frac{1}{r} \frac{\partial v}{\partial \theta}, \quad (6)$$

$$\gamma_{r\theta} = -\frac{\nu}{r} + \frac{\partial \nu}{\partial r} = 0. \quad (7)$$

the equilibrium equation is;

$$\sigma_{\theta} = \frac{d}{dr}(r\sigma_r) \quad (8)$$

Taking into account a variable modulus of elasticity $E = E(r)$ and a variable coefficient of thermal expansion $\alpha = \alpha(r)$, but Poisson's ratio (ν) constant, the generalized Hooke's law can be given as;

$$\varepsilon_r = \frac{1}{E(r)} [\sigma_r - \nu(\sigma_{\theta} + \sigma_z)] + \alpha(r)T, \quad (9)$$

$$\varepsilon_{\theta} = \frac{1}{E(r)} [\sigma_{\theta} - \nu(\sigma_r - \sigma_z)] + \alpha(r)T, \quad (10)$$

$$\varepsilon_z = 0 = \frac{1}{E(r)} [\sigma_z - \nu(\sigma_r + \sigma_{\theta})] + \alpha(r)T. \quad (11)$$

In order to describe the material properties at any point of the curved FGM beam, general linear mixture law is used. The general linear rule of mixture reads

$$\text{Pr}_{eff}(r) = \text{Pr}_0 V_0(r) + \text{Pr}_1 V_1(r) \quad (12)$$

where Pr_{eff} denotes material property, and subscripts 0 (zero) and 1 specifies the volume fraction of material. In addition, It has been suggested that there are pure components on the inner surface of the

curved beam, 0 (zero) of the curved FGM beam, i.e., $V_0(a) = 1$ and with the index 1 indicating the second constituent, it is given as;

$$V_1(r) = 1 - V_0(r). \quad (13)$$

The modulus of elasticity is as follows:

$$E(r) = E_0 \left(\frac{r}{a} \right)^m, \quad (14)$$

Eqs. (13) and (14) are substituted in Eq. (12) and a straight forward the relation of the volume fraction coefficient of the constituent 0 are obtained.

$$V_0(r) = \frac{E_0 \left(\frac{r}{a} \right)^m - E_1}{E_0 - E_1} \quad (15)$$

Then, applying the rule of mixture Eq.12, the coefficient of thermal expansion $\alpha(r)$ and the density $\rho(r)$, the uniaxial yield limit $\sigma_y(r)$, and the thermal conductivity $k(r)$, respectively, one obtains

$$Pr_{eff}(r) = A_{Pr} \left(\frac{r}{a} \right)^m + B_{Pr} \quad (16)$$

with

$$A_{Pr} = \frac{E_0 (Pr_0 - Pr_1)}{E_0 - E_1}, \quad B_{Pr} = \frac{E_0 Pr_1 - E_1 Pr_0}{E_0 - E_1} \quad (17)$$

where $Pr = \alpha, \rho, \sigma_y,$ and k , respectively. It is assumed that the Poisson's ratio ν is assumed to be constant. The properties of materials are connected to the radial coordinate.

Basic equations for FGM beam can be obtained. First, using Eqs. (11), (14), (16), (17) and $\varepsilon_z = 0$, the axial stress as follows

$$\sigma_z = \nu(\sigma_r + \sigma_\theta) - E_0 \left(\frac{r}{a}\right)^m \left[\left(A_\alpha \left(\frac{r}{a}\right)^m + B_\alpha \right) T \right]. \quad (18)$$

integration of relation (7) gives

$$\nu = rf \quad (19)$$

where f is a function of θ only. Then, differentiating Eq. (6) with respect to θ and taking into account that both θ and u depend on r only, one obtains

$$\frac{\partial^2 \nu}{\partial \theta^2} = 0 \quad (20)$$

and hence;

$$\nu = C_1 r \theta \quad (21)$$

with the (non-dimensional) constant of integration C_1 . Hence, based on Eqs. (5), (6), and Hooke's law (9), (10), σ_r , and σ_θ can be expressed in terms of u and its derivative with respect to r (denoted by a prime),

$$\sigma_r = \frac{E_0 \left(\frac{r}{a}\right)^m}{(1+\nu)(1-2\nu)} \left[\begin{array}{l} \frac{\nu u}{r} + (1-\nu)u' + \nu C_1 \\ -(1+\nu) \left(A_\alpha \left(\frac{r}{a}\right)^m + B_\alpha \right) T \end{array} \right], \quad (22)$$

$$\sigma_{\theta} = \frac{E_0 \left(\frac{r}{a}\right)^m}{(1-2\nu)} \left[\begin{array}{l} \frac{(1-\nu)u}{(1+\nu)r} + \frac{C_1(1-\nu)+\nu u'}{1+\nu} \\ - \left(A_{\alpha} \left(\frac{r}{a}\right)^m + B_{\alpha} \right) T \end{array} \right]. \quad (23)$$

Eqs. (22) and (23) are substituted in Eq. (8) to obtain the differential equation for displacement.

$$\begin{aligned} & r^{1+m}u'' + (1+m)r^m u' - \frac{r^{-1+m} [1-\nu(1+m)]u}{1-\nu} \\ &= \frac{r^m}{1-\nu} \left[\begin{array}{l} C_1 [1-\nu(2+m)] + m \left(2A_{\alpha} \left(\frac{r}{a}\right)^m + B_{\alpha} \right) \\ \times (1+\nu)T + r \left(A_{\alpha} \left(\frac{r}{a}\right)^m + B_{\alpha} \right) (1+\nu)T' \end{array} \right] \end{aligned} \quad (24)$$

Its solution is

$$\begin{aligned} u &= C_2 r^{(-m+S)/2} + C_3 r^{(-m-S)/2} + \frac{C_1 r [1-\nu(2+m)]}{m} \\ & - \frac{1+\nu}{2S(1-\nu)a^m r^{(m+S)/2}} \\ & \times \left[\begin{array}{l} (2-m-S)r^S \left(a^m B_{\alpha} \int_a^r \xi^{(m-S)/2} T d\xi + A_{\alpha} \int_a^r \xi^{(3m-S)/2} T d\xi \right) \\ - (2-m+S) \left(a^m B_{\alpha} \int_a^r \xi^{(m+S)/2} T d\xi + A_{\alpha} \int_a^r \xi^{(3m+S)/2} T d\xi \right) \end{array} \right] \end{aligned} \quad (25)$$

where C_2 and C_3 are constants of integration, and

$$S = \sqrt{4 + m^2 - \frac{4m\nu}{1-\nu}} \quad (26)$$

Thereof, solving Eqs. (22) and (23), one finally obtains

$$\sigma_r = \frac{C_1 E_0 \left(\frac{r}{a}\right)^m}{m(1+\nu)} + \frac{E_0 r^{(-2+m-S)/2}}{2a^m(1+\nu)(1-2\nu)} \times \left\{ C_3 \left[(2+m+S)\nu - m - S \right] + C_2 r^S \left[(2+m-S)\nu - m + S \right] \right\} + \frac{E_0 r^{(-2+m-S)/2}}{2Sa^{2m}(1-\nu)} \left[(2+m-S)r^S \left(a^m B_\alpha \int_a^r \xi^{(m-S)/2} T d\xi + A_\alpha \int_a^r \xi^{(3m-S)/2} T d\xi \right) - (2+m+S) \left(a^m B_\alpha \int_a^r \xi^{(m+S)/2} T d\xi + A_\alpha \int_a^r \xi^{(3m+S)/2} T d\xi \right) \right] \quad (27)$$

$$\sigma_\theta = \frac{C_1 E_0 (1+m) \left(\frac{r}{a}\right)}{m(1+\nu)} - \frac{E_0 \left\{ C_3 r^{(-2+m+S)/2} \left[(2+m+S)\nu - 2 \right] + C_2 r^{(-2+m-S)/2} \left[(2+m-S)\nu - 2 \right] \right\}}{2(1+\nu)(1-2\nu)a^m} + \frac{E_0 r^{(-2+m-S)/2}}{4S(1+\nu)(1-2\nu)a^{2m}} \times \left\{ r^S \left[(m+S-2)(2+(S-m-2)\nu) \right] \left(a^m B_\alpha \int_a^r \xi^{(m-S)/2} T d\xi + A_\alpha \int_a^r \xi^{(3m-S)/2} T d\xi \right) + \left[(m-S-2)(-2+(2+m+S)\nu) \right] \left(a^m B_\alpha \int_a^r \xi^{(m+S)/2} T d\xi + A_\alpha \int_a^r \xi^{(3m+S)/2} T d\xi \right) \right\} - 4Sr^{(2+m+S)/2} (a^m B_\alpha + r^m A_\alpha) (1-2\nu) T \quad (28)$$

and σ_z obtained from Eq. (18).

In the above basic equations, the three constants of integration, C_1 , C_2 and C_3 , must be determined. For the determination of these unknowns, the conditions Eqs. (1) - (3) are available. These conditions lead to

$$C_1 = \frac{m(1+\nu)(1-2\nu)}{a^m L_1 (1-\nu) S} \times \left\{ 2L_3 (a^s - b^s) + L_2 \left[a^s (m-S-(2+m-S)\nu) - r_0^s (m+S-(2+m+S)\nu) \right] \right\} \quad (29)$$

$$C_2 = \frac{(1+\nu)}{2a^m L_1 (1-\nu) S \left\{ a^S [m-S-(2+m-S)\nu] - r_0^S [m+S-(2+m+S)\nu] \right\}} \times \left\{ [m+S-(2+m+S)\nu] L_1 L_3 + 2 \left[2a^{(2+m+S)/2} (1-2\nu) + r_0^{(2+m+S)/2} [1-(2+m)\nu] [m+S-(2+m+S)\nu] \right] \times (1-2\nu) \left\{ 2L_3 (a^S - b^S) + L_2 [r_0^S [m+S-(2+m+S)\nu] - a^S [m-S-(2+m-S)\nu]] \right\} \right\} \quad (30)$$

$$C_3 = \frac{a^{(-2m+S)/2} (1+\nu)}{2SL_1 (1-\nu) \left\{ a^S [m-S-(2+m-S)\nu] - r_0^S [m+S-(2+m+S)\nu] \right\}} \times \left\{ a^{S/2} [m-S-(2+m-S)\nu] L_1 L_3 - 2r_0^{S/2} \left[2a^{(2+m)/2} (1-2\nu) + a^{S/2} [1-(2+m)\nu] [m-S-(2+m-S)\nu] \right] \times (1-2\nu) \left\{ 2L_3 (a^S - b^S) + L_2 [a^S [m-S-(2+m-S)\nu] - r_0^S [m+S-(2+m+S)\nu]] \right\} \right\} \quad (31)$$

where;

$$L_1 = \left\{ b^S [m-S-(2+m-S)\nu] - r_0^S [m+S-(2+m+S)\nu] \right\} \times \left\{ 2a^{(2+m+S)/2} (1-2\nu) + r_0^{(2+m+S)/2} [1-(2+m)\nu] [m+S-(2+m+S)\nu] \right\} - \left\{ a^S [m-S-(2+m-S)\nu] - r_0^S [m+S-(2+m+S)\nu] \right\} \times \left\{ 2b^{(2+m+S)/2} (1-2\nu) + r_0^{(2+m+S)/2} [1-(2+m)\nu] [m+S-(2+m+S)\nu] \right\} \quad (32)$$

$$L_2 = b^S (2-m-S) \left[a^m B_\alpha \int_a^b r^{(m-S)/2} T dr + A_\alpha \int_a^b r^{(3m-S)/2} T dr \right] - (2+m+S) \left[a^m B_\alpha \int_a^b r^{(m+S)/2} T dr + A_\alpha \int_a^b r^{(3m+S)/2} T dr \right] \quad (33)$$

$$L_3 = r_0^S (2-m-S) \left[a^m B_\alpha \int_a^{r_0} r^{(m-S)/2} T dr + A_\alpha \int_a^{r_0} r^{(3m-S)/2} T dr \right] - (2-m+S) \left[a^m B_\alpha \int_a^{r_0} r^{(m+S)/2} T dr + A_\alpha \int_a^{r_0} r^{(3m+S)/2} T dr \right] \quad (34)$$

In this way, after the temperature field is determined, the strain and stress in the beam can be known. Furthermore, by substituting the circumferential stress σ_θ given in Eqs. (28) and (4), couple moment M is expressed as follows;

$$\begin{aligned}
 M = & \frac{E_0}{a^m(1+\nu)} \left\{ \frac{C_1(1+m)}{m(2+m)} (b^{2+m} - a^{2+m}) + \frac{C_2[(2+m-S)\nu - 2]}{(2+m+S)(1-2\nu)} \right. \\
 & \times \left(a^{(2+m+S)/2} - b^{(2+m+S)/2} \right) - \frac{C_3[(2+m+S)\nu - 2]}{(2+m-S)(1-2\nu)} \left(a^{(2+m-S)/2} - b^{(2+m-S)/2} \right) \left. \right\} \\
 & + \frac{E_0}{2Sa^{2m}(1-\nu)^2} \left\{ [m+S-2+(2+m-S)\nu] \right. \\
 & \times \left[a^m B_\alpha \int_a^b r^{(m+S)/2} \left(\int_a^r \xi^{(m-S)/2} T d\xi \right) dr + A_\alpha \int_a^b r^{(m+S)/2} \left(\int_a^r \xi^{(3m-S)/2} T d\xi \right) dr \right] \\
 & + [2-m+S-(2+m+S)\nu] \\
 & \times \left[a^m B_\alpha \int_a^b r^{(m-S)/2} \left(\int_a^r \xi^{(m+S)/2} T d\xi \right) dr + A_\alpha \int_a^b r^{(m-S)/2} \left(\int_a^r \xi^{(3m+S)/2} T d\xi \right) dr \right] \left. \right\} \\
 & - \frac{E_0}{a^{2m}(1-\nu)} \left(B_\alpha \int_a^b r^{1+m} T dr + A_\alpha \int_a^b r^{1+2m} T dr \right).
 \end{aligned} \tag{35}$$

Temperature Field

When the temperature change is regarded as steady state, the temperature increase of inner or outer surfaces is thought to increase slowly and is calculated independently from time. In this case, it is governed the differential equation by Peng and Li (2010).

$$\frac{1}{r} \frac{d}{dr} \left[rk(r) \frac{dT(r)}{dr} \right] = 0 \quad (36)$$

With the dependence of the thermal conductivity on the radius given by Eqs. (16) and (17), its solution is

$$T(r) = \frac{D_1 \left\{ m \ln(r) - \ln \left[A_k \left(\frac{r}{a} \right)^m + B_k \right] \right\}}{mB_k} + D_2 \quad (37)$$

where D_1 and D_2 are constants of integration. When the surface temperature at the inner and outer sides is prescribed as;

$$T(a) = T_a \quad T(b) = T_b \quad (38)$$

and give rise to

$$T(r) = \frac{\left\{ m \ln(r/b) + \ln \left[A_k (b/a)^m + B_k \right] - \ln \left[A_k (r/a)^m + B_k \right] \right\} T_a}{-m \ln(b/a) - \ln \left[A_k + B_k \right] + \ln \left[A_k (b/a)^m + B_k \right]} + \frac{\left\{ -m \ln(r/a) + \ln \left[A_k (r/a)^m + B_k \right] - \ln \left[A_k + B_k \right] \right\} T_b}{-m \ln(b/a) - \ln \left[A_k + B_k \right] + \ln \left[A_k (b/a)^m + B_k \right]}. \quad (39)$$

Stress Distributions and Effect of Exponential Parameter

With the equations obtained above, the stresses can be calculated. The von Mises yield criterion was used to determine the elastic limits and as follows;

$$\sigma_M(r) = \sigma_y(r), \quad \sigma_M = \sqrt{\frac{1}{2} [(\sigma_r - \sigma_\theta)^2 + (\sigma_\theta - \sigma_z)^2 + (\sigma_z - \sigma_r)^2]}. \quad (40)$$

Now, introducing the following non-dimensional quantities:

$$\bar{k} = \frac{k}{k_0}, \quad \bar{r} = \frac{r}{a}, \quad \bar{E} = \frac{E}{E_0}, \quad \bar{M} = \frac{M}{a^2 \sigma_{y,0}} \quad (41)$$

$$\bar{T} = \frac{\alpha_0 E_0 T}{\sigma_{y,0}}, \quad \bar{\alpha} = \frac{\alpha}{\alpha_0}, \quad \bar{\sigma}_i = \frac{\sigma_i}{\sigma_{y,0}}, \quad \bar{\rho} = \frac{\rho}{\rho_0} \quad (42)$$

where, it should be remembered that the pure FGM component of index 0, $r = a$, represents a material parameter. The exponential grading index m_{ext} in the curved FGM beam is as follows;

$$m_{ext} = \frac{\ln(\bar{E}_1)}{\ln(b)}. \quad (43)$$

Thus, depending on whether $E_1 > 1$ or $E_1 < 1$, there hold the relations $0 < m \leq m_{ext}$ or $m_{ext} \leq m < 0$ respectively. To calculate numerically these equations, material properties and surface radius ratios are specified. In particular, a beam with radii ratio $b/a = 1.25$, Poisson's ratio $\nu = 0.3$, and $E_1/E_0 = 0.35$, $\alpha_1/\alpha_0 = 1.39$, $k_1/k_0 = 4.75$, $\sigma_{y,1}/\sigma_{y,0} = 0.15$, $\rho_1/\rho_0 = 0.35$ is considered. These values correspond to an FGM composed of steel (index 0) and aluminum (index 1) with pure steel at $r = a$ (e.g. Nemat-Alla, 2011). The corresponding extremum value for

the grading exponent is $m = m_{\text{exp}} = -4.705$. Fig. 2 shows the temperature distribution and the modulus of elasticity corresponding to different exponential parameter values.

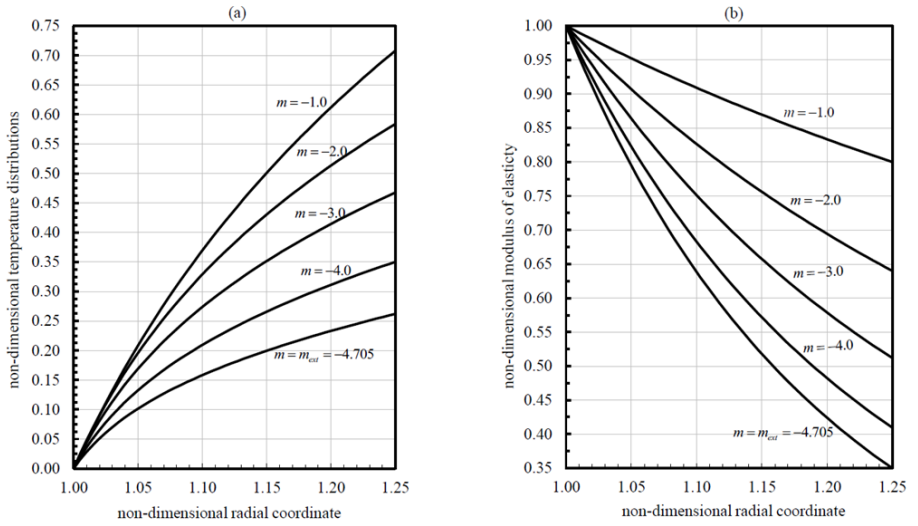


Figure 2. Distribution for various m - values (a) positive temperature gradients (b) modulus of elasticity

Positive Temperature Gradient

Elastic behavior of the steel/aluminum cylindrically curved FGM beam have been investigated analytically. Stress distributions are calculated according to different surface temperature conditions. These surface temperature differences ($\Delta T = T_b - T_a$) have been investigated in accordance with the exponential parameter m , $\Delta T > 0$ and $\Delta T < 0$. Figs. 3 presents the stresses and elastic limit values of the homogeneous beam and three different grading exponents. Homogeneous beam made of steel and appears to yield on the outer surface for $m = -10^{-7}$, $\bar{T}_a = 0$ and $\Delta \bar{T} = 0.982$ positive temperature with a homogeneous curved beam, see Fig. 3a. Figure 3b shows for $m = -1.60$, $\bar{T}_a = 0$ and $\Delta \bar{T} = 0.729$ the elastic limits in the curved FGM beam. The volume ratio of the steel on the outer surface of the curved FGM beam is calculated as 53.8% and the volume fraction ratio of aluminum as 46.2%. The onset of the yield would occur at the outer surface of curved FGM beam. Figure 3c presents for $m = -2.40$, $\bar{T}_a = 0$ and $\Delta \bar{T} = 0.620$ the elastic limits in the beam. The volume fraction ratio of the steel on the outer surface of the beam is calculated as 36.2% and the volume ratio of aluminum as 63.8%. The onset of the yield would occur at the outer surface of beam. Figure 3d shows for $m = m_{ext} = -4.705$, $\bar{T}_a = 0$ and $\Delta \bar{T} = 0.302$ the elastic limits in the beam. The volume ratio of the steel on the outer surface of the beam is calculated as 0% and the volume ratio of aluminum as 100%. The onset of the yield would occur at the outer surface of beam.

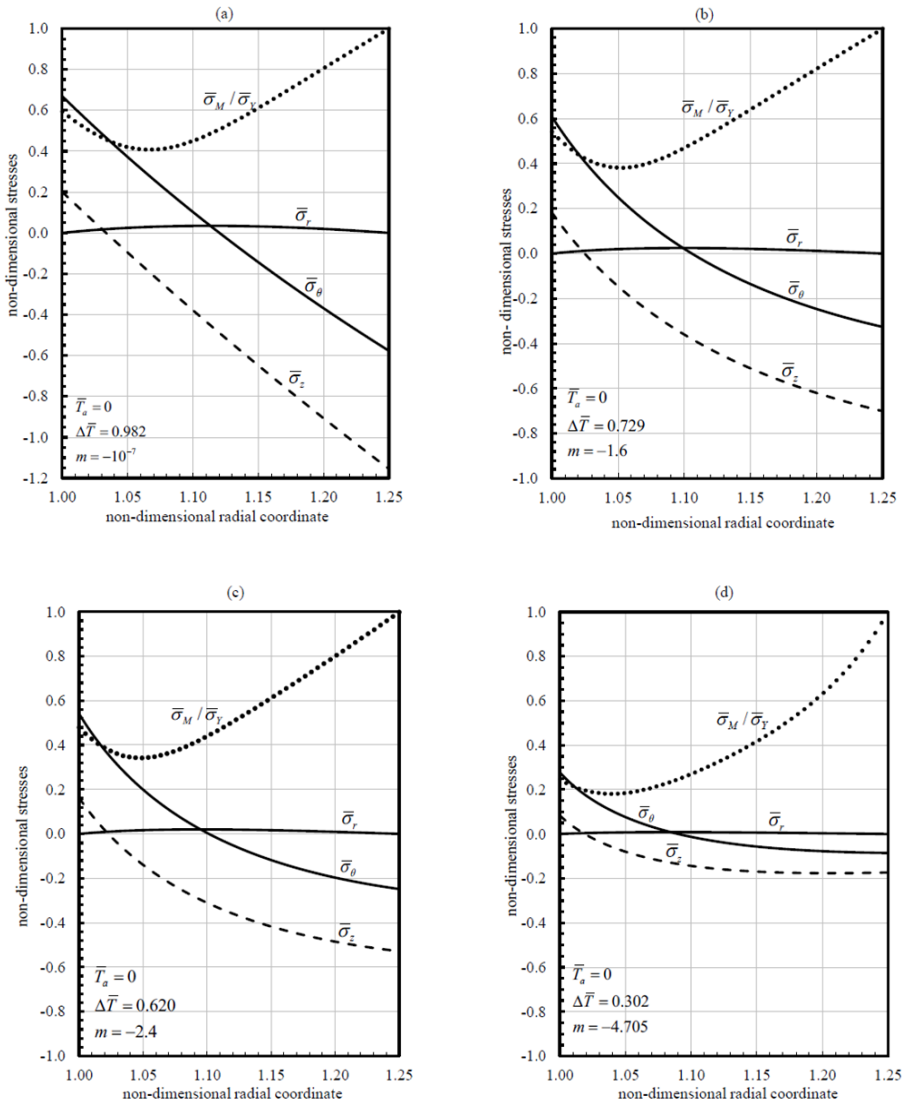


Figure 3. Elastic behavior and stress distributions for positive temperature gradient and various m - parameter **a)** $m = -10^{-7}$ **b)** $m = -1.60$ **c)** $m = -2.40$ **d)** $m = m_{\text{exp}} = -4.705$

Negative temperature gradient

Figure 4 presents the stress distributions for a homogeneous beam and three different m - parameter for $\Delta T < 0$, i.e, an increased inner surface temperature. Homogeneous beam made of steel and appears to yield on the outer surface for $m = -10^{-7}$, $\bar{T}_a = 0.900$ and $\Delta\bar{T} = -0.900$ negative temperature with a homogeneous curved beam (see Figure 4a). Figure 4b shows for $m = -1.60$, $\bar{T}_a = 0.893$ and $\Delta\bar{T} = -0.893$ the elastic limits and stress distributions in the curved FGM beam. The onset of the yield would occur at the inner surface of curved FGM beam. Figure 4c depicts for $m_{cr}^n = -3.761$, $\bar{T}_a = 0.911$ and $\Delta\bar{T} = -0.911$ the elastic limits and stress distributions in the curved FGM beam. At the negative temperature and at the critical value m_{cr}^n , yield occurs simultaneously on both the inner and outer surfaces of the beam. Figure 4d shows for $m = m_{ext} = -4.705$, $\bar{T}_a = 0.631$ and $\Delta\bar{T} = -0.631$ the elastic limits and stress distributions in the curved FGM beam. The onset of the yield would occur at the outer surface of beam. The elastic behavior and stress distributions corresponding to the m - values and occurring in the curved FGM beam for different temperature conditions are detailed in Figure 5.

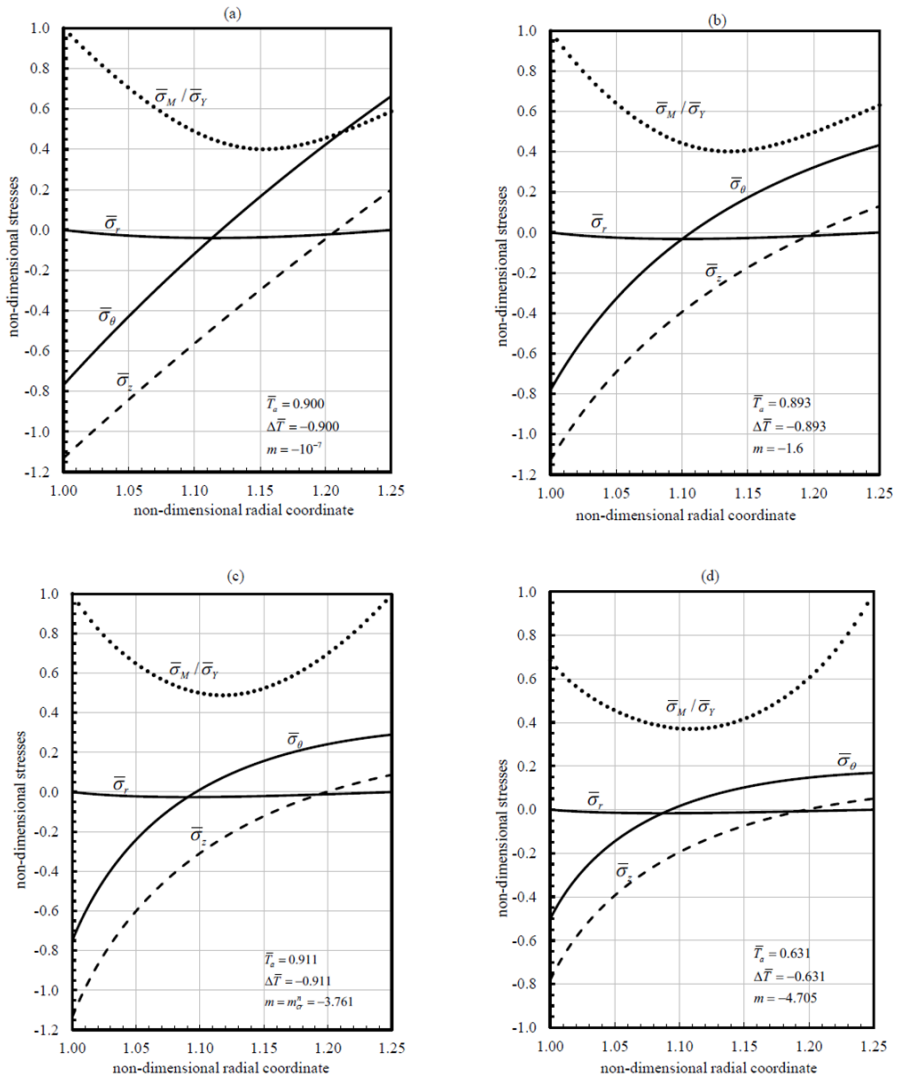


Figure 4. Elastic behavior and stress distributions for negative temperature gradient and various m - parameter **a)** $m = -10^{-7}$ **b)** $m = -1.60$ **c)** $m = m_{cr}^n = -3.761$ **d)** $m = m_{exp} = -4.705$

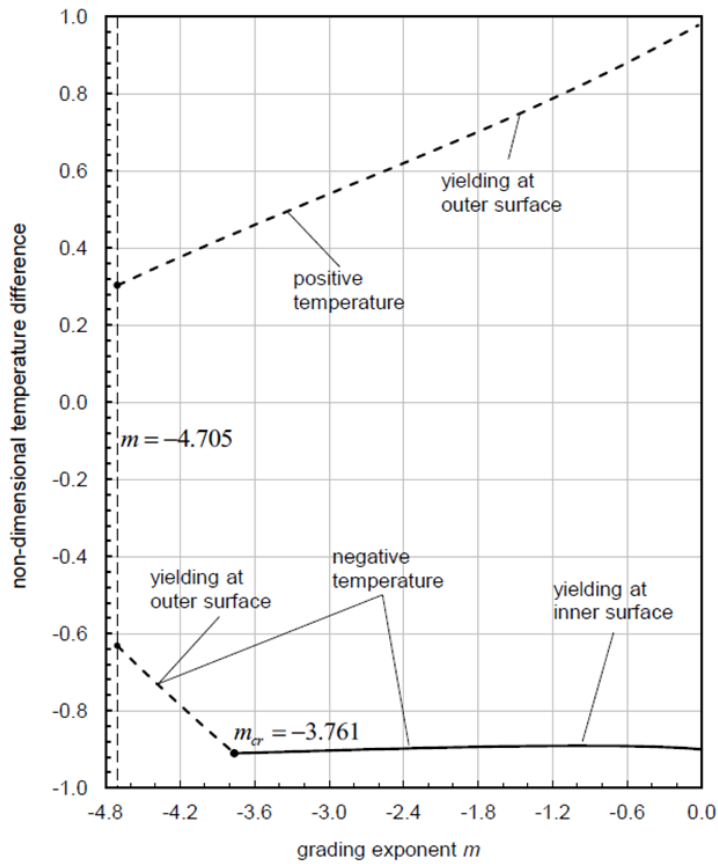


Figure 5. Temperature difference at the elastic behavior vs. m - parameter for $\Delta \bar{T} > 0$ and $\Delta \bar{T} < 0$

CONCLUSION

In this study, an analytical solution is investigated the elastic behavior and stress distributions of the Steel/Aluminum curved FGM beam in the plane strain state under temperature grading in radial direction. It is considered that the temperature distribution changes as a function of the radial coordinate and is in steady state. The modulus of elasticity varies with the thickness of the beam according to the power law. Accordingly, by applying the general mixture law, the thermal expansion coefficient, the thermal conductivity coefficient, uniaxial yield stress and the volume fraction vary depending on the power law (except Poisson's ratio).

In the positive temperature distribution, the yield in the curved FGM beam occurs on the outer surface. But in the negative temperature distribution, the yield in the curved FGM beam is on the inner surface until the critical value of $m = m_{cr}^n$ and the yield occurs on the outer surface for $m < m_{cr}^n$. Of course, the outer surface of the beam should not be ignored.

The equations obtained above can be applied in a different FGMs component.

Finally, although the above-mentioned closed-form solution requires certain assumptions for boundary conditions, it is quite striking that the remaining numerical effort is limited to the integration of the terms that contain mainly the analytically derived temperature field.

REFERENCES

- Arslan, E., & Eraslan, A. N. (2010). Analytical solution to the bending of a nonlinearly hardening wide curved bar. *Acta Mechanica*, 210(1-2), 71-84.
- Arslan, E., & Mack, W. (2014). Elastic-plastic states of a radially heated thick-walled cylindrically curved panel. *Forschung im Ingenieurwesen*, 78(1-2), 1-11.
- Arslan, E., & Mack, W. (2015). Shrink fit with solid inclusion and functionally graded hub. *Composite Structures*, 121, 217-224.
- Awaji, H., & Sivakumar, R. (2001). Temperature and Stress Distributions in a Hollow Cylinder of Functionally Graded Material: The Case of Temperature - Independent Material Properties. *Journal of the American Ceramic Society*, 84(5), 1059-1065.
- Birman, V., & Byrd, L. W. (2007). Modeling and analysis of functionally graded materials and structures. *Applied mechanics reviews*, 60(5), 195-216.
- Dadras, P. (2001). Plane strain elastic-plastic bending of a strain-hardening curved beam. *International journal of mechanical sciences*, 43(1), 39-56.

- Dryden, J. (2007). Bending of inhomogeneous curved bars. *International Journal of Solids and Structures*, 44(11-12), 4158-4166.
- Duc, N. D., & Van Tung, H. (2010). Nonlinear response of pressure-loaded functionally graded cylindrical panels with temperature effects. *Composite Structures*, 92(7), 1664-1672.
- Eraslan, A. N., & Akis, T. (2006). On the plane strain and plane stress solutions of functionally graded rotating solid shaft and solid disk problems. *Acta Mechanica*, 181(1-2), 43-63.
- Eraslan, A. N., & Arslan, E. (2008). A concise analytical treatment of elastic - plastic bending of a strain hardening curved beam. *ZAMM - Journal of Applied Mathematics and Mechanics/Zeitschrift für Angewandte Mathematik und Mechanik: Applied Mathematics and Mechanics*, 88(8), 600-616.
- Evcı, C., & Gülgeç, M. (2018). Functionally graded hollow cylinder under pressure and thermal loading: Effect of material parameters on stress and temperature distributions. *International Journal of Engineering Science*, 123, 92-108.
- Kiani, Y., Shakeri, M., & Eslami, M. R. (2012). Thermoelastic free vibration and dynamic behaviour of an FGM doubly curved panel via the analytical hybrid Laplace–Fourier transformation. *Acta Mechanica*, 223(6), 1199-1218.

- Librescu, L., Nemeth, M. P., Starnes Jr, J. H., & Lin, W. (2000). Nonlinear response of flat and curved panels subjected to thermomechanical loads. *Journal of thermal stresses*, 23(6), 549-582.
- Mohammadi, M., & Dryden, J. R. (2008). Thermal stress in a nonhomogeneous curved beam. *Journal of Thermal Stresses*, 31(7), 587-598.
- Naebe, M., & Shirvanimoghaddam, K. (2016). Functionally graded materials: A review of fabrication and properties. *Applied Materials Today*, 5, 223-245.
- Nemat-Alla, M. M., Ata, M. H., Bayoumi, M. R., & Khair-Eldeen, W. (2011). Powder metallurgical fabrication and microstructural investigations of aluminum/steel functionally graded material. *Materials Sciences and Applications*, 2(12), 1708.
- Noda, N. (1999). Thermal stresses in functionally graded materials. *Journal of Thermal Stresses*, 22(4-5), 477-512.
- Peng, X. L., & Li, X. F. (2010). Thermal stress in rotating functionally graded hollow circular disks. *Composite Structures*, 92(8), 1896-1904.
- Shaffer, B. W., & House Jr, R. N. (1957). Displacements in a wide curved bar subjected to pure elastic-plastic bending. *J. Appl. Mech. Trans. ASME*, 24, 447-452.

Shaffer, B. W., & House, R. N. (1954). *The elastic-plastic stress distribution within a wide curved bar subjected to pure bending*. New York Univ Bronx School Of Engineering And Science.

Shao, Z. S. (2005). Mechanical and thermal stresses of a functionally graded circular hollow cylinder with finite length. *International Journal of Pressure Vessels and Piping*, 82(3), 155-163.

Sobczak, J. J., & Drenchev, L. (2013). Metallic functionally graded materials: a specific class of advanced composites. *Journal of Materials Science & Technology*, 29(4), 297-316.

Timoshenko, S.P. and Goodier J.N. (1970) *Theory of Elasticity*, 3rd ed., McGraw-Hill, New York.

Zimmerman, R. W., & Lutz, M. P. (1999). Thermal stresses and thermal expansion in a uniformly heated functionally graded cylinder. *Journal of Thermal Stresses*, 22(2), 177-188.

CHAPTER 3
**FREE VIBRATION ANALYSIS OF A CRACKED
BEAM WITH VARIABLE CROSS SECTION**

Assist Prof. Mehmet HASKUL¹

Prof. Murat KISA²

¹ Sirnak University, Faculty of Engineering, Department of Mechanical Engineering, Sirnak, Turkey. mehmethaskul@sirnak.edu.tr

² Harran University, Faculty of Engineering, Department of Mechanical Engineering, Sanliurfa, Turkey. mkisa@harran.edu.tr

INTRODUCTION

In this study, a numerical method for the free vibration analysis of a cracked non uniform beam is presented. It is assumed that the width of the beam is constant and its thickness varies linearly. Finite element method is used to find the modal data of the cracked non uniform beam. The crack in the beam is modeled as a massless spring. It is evident that a structural defect such as a crack results in a decrease in the overall stiffness of the structure. Stiffness drops due to the cracks are derived from the fracture mechanics theory as the inverse of the compliance matrix calculated with the proper stress intensity factors and strain energy release rate expressions. The effects of the crack location, crack depth and thickness ratios on natural frequencies and mode shapes are investigated by giving several examples. The method given by the current study can be used for the free vibration analysis of cracked beams with variable cross sections.

Non uniform cross-section beams are found in many machines and construction structures. Amirikian (1972) first mentioned the importance of the variable cross-section structures. An approximate method for determining static displacements and moments in straight or variable cross-section beams was developed by Newmark (1943). Finite difference and finite element methods are the leading methods for the analysis of varying cross-section beams (Ghali and Neville, 1972; Martin, 1966). Rissone and Williams (1965) performed a detailed frequency analysis of variable section beams using finite difference method using Euler and Timoshenko beam theories.

Studies on the variable cross-section beams with cracks are important and found to be insufficient in the literature. Just (1975, 1977) developed the stiffness matrix of variable cross section beams. Free vibration analysis of non-uniform structures was performed by various methods such as perturbation technique (Martin (1956)), Euler and Timoshenko beam theories (Gaines and Volterra (1966, 1968)) and Rayleigh-Ritz method (Klein (1974)). Thomas and Dokumacı (1973) developed a varying cross-section beam element using sixth Hermitian polynomials. Kolousek (1973) developed a dynamic stiffness matrix of a beam element with a general variable section. Avakian and Bestos (1976) investigated the free vibration problem of general and nonlinear variable cross-section beams using dynamic stiffness matrices. Karabalis and Bestos (1983) proposed a numerical method that can perform static, dynamic and stability analysis of the beams with constant width and variable thickness. Takahashi (1998) used the transfer matrix method to analyze the buckling and vibration of axially loaded variable cross-section columns with a crack. Franciosi and Mecca (1998) proposed three types of finite elements for the static analysis of the variable section beams. The performance of these elements was shown by various examples and it was proven that the elements were safe. Al-Gahtani and Khan (1998) developed a method of analysis for the general boundary conditions of non-prismatic beams. Zheng and Fan (2001) found the natural frequencies of a multi-cracked beam with a variable cross section using the Fourier series. Li (2002) conducted the free vibration analysis of multiple cracked beam. He modeled the regional flexibility with a massless spring due to the crack

in the cross-section. Ruta (2002) developed a dynamic stiffness matrix of variable cross-section bars on elastic foundation. Mazanoğlu and Sabuncu (2010) investigated the bending vibration of non-uniform rectangular beams with multiple edge cracks along the beam's height. Bayat et al. (2011) investigated the nonlinear free vibrations of beams. In the study the governing equation of the nonlinear, large amplitude free vibrations of tapered beams were derived.

A new implementation of the ancient Chinese method called the Max-Min Approach (MMA) and Homotopy Perturbation Method (HPM) are presented to obtain natural frequency and corresponding mode shapes of tapered beams. Tan et al. (2018) proposed an approach to investigate the free vibration of cracked non-uniform beam with general boundary conditions. One of the advantages of the proposed method was that it can be used to assess the free vibration of the cracked non-uniform beams with any variable cross-section form represented by the polynomial distribution.

MATHEMATICAL MODELING

Stiffness and Mass Matrices of the Beam with Constant Width and Variable Thickness.

In this study, free vibration analysis of a cracked beam with variable cross section is performed utilizing the Finite Element Method. Firstly, for the modelling of whole beam, the stiffness and mass matrices of a beam element with two nodes and three degrees of freedom at the each node are derived(Figure 1).

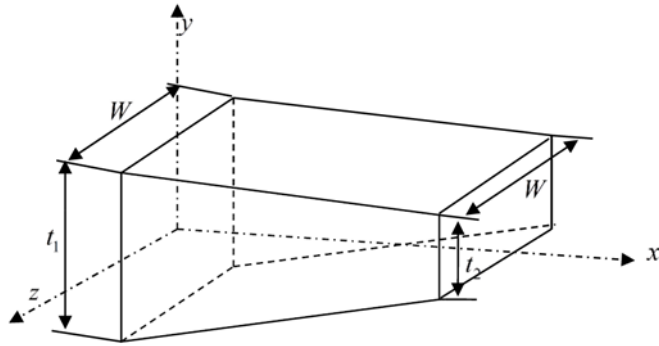


Figure 1. A beam with constant width and variable thickness
Flexural ($EI_{zz}(x)$) and axial ($EA(x)$) rigidities at the distance x from the left end can be given as follows (Friedman and Kosmatka, 1992);

$$EI_{zz}(x) = EI_{zz1} \left(1 + \alpha \left(\frac{x}{L} \right) \right)^3 \quad (1)$$

$$EA(x) = EA_1 \left(1 + \alpha \left(\frac{x}{L} \right) \right) \quad (2)$$

where $I_{zz}(x)$, $A(x)$ indicate the moment of inertia and cross-sectional area at left end respectively, L is the beam length. α is given by,

$$\alpha = \frac{t_2 - t_1}{t_1} \quad (3)$$

where t_1 and t_2 indicate the thicknesses at the left and right ends, respectively.

The stiffness matrix of the beam element with constant width and variable thickness is given as follows (Haskul, 2010).

$$K = \begin{bmatrix} \frac{1}{C} & 0 & 0 & \frac{-1}{C} & 0 & 0 \\ 0 & \frac{A_1}{D_1} & \frac{A_2}{D_1} & 0 & \frac{-A_1}{D_1} & \frac{A_1L - A_2}{D_1} \\ 0 & \frac{A_2}{D_1} & \frac{A_3}{D_1} & 0 & \frac{-A_2}{D_1} & \frac{A_2L - A_3}{D_1} \\ \frac{-1}{C} & 0 & 0 & \frac{1}{C} & 0 & 0 \\ 0 & \frac{-A_1}{D_1} & \frac{-A_2}{D_1} & 0 & \frac{A_1}{D_1} & \frac{A_2 - A_1L}{D_1} \\ 0 & \frac{A_1L - A_2}{D_1} & \frac{A_2L - A_3}{D_1} & 0 & \frac{A_2 - A_1L}{D_1} & \frac{A_1L^2 - 2A_2L + A_3}{D_1} \end{bmatrix} \quad (4)$$

where the terms A_1 , A_2 , A_3 , D_1 and C are given as follows (Haskul, 2010);

$$A_i = \int_0^L \frac{x^{(i-1)}}{EI_{zz}(x)} dx, \quad i = 1, 2, 3 \quad (5)$$

$$D_1 = A_1 \cdot A_3 - A_2^2 \quad (6)$$

$$\frac{1}{C} = \frac{EA_1}{L} \left[\frac{\alpha}{\ln(\alpha + 1)} \right] \quad (7)$$

The mass matrix of the beam element with constant width and linearly varying thickness can be given as (Haskul, 2010).

$$[M] = \begin{bmatrix} m_{11}^A & 0 & 0 & m_{12}^A & 0 & 0 \\ 0 & m_{11}^B & m_{12}^B & 0 & m_{13}^B & m_{14}^B \\ 0 & m_{21}^B & m_{22}^B & 0 & m_{23}^B & m_{24}^B \\ m_{21}^A & 0 & 0 & m_{22}^A & 0 & 0 \\ 0 & m_{31}^B & m_{32}^B & 0 & m_{33}^B & m_{34}^B \\ 0 & m_{41}^B & m_{42}^B & 0 & m_{43}^B & m_{44}^B \end{bmatrix}_{6 \times 6} \quad (8)$$

where the terms m_{ij}^A and m_{ij}^B are (Haskul, 2010);

$$[m]^A = \begin{bmatrix} \frac{1}{12} \rho A_1 L (4 + \alpha) & \frac{1}{12} \rho A_1 L (2 + \alpha) \\ \frac{1}{12} \rho A_1 L (2 + \alpha) & \frac{1}{12} \rho A_1 L (4 + 3\alpha) \end{bmatrix} \quad (9)$$

$$[m]^B = \begin{bmatrix} \frac{1}{35} \rho A_1 L (13 + 3\alpha) & \frac{1}{420} \rho A_1 L^2 (22 + 7\alpha) & \frac{9}{140} \rho A_1 L (2 + \alpha) & -\frac{1}{420} \rho A_1 L^2 (13 + 6\alpha) \\ & \frac{1}{840} \rho A_1 L^3 (8 + 3\alpha) & \frac{1}{420} \rho A_1 L^2 (13 + 7\alpha) & -\frac{1}{280} \rho A_1 L^3 (2 + \alpha) \\ & & \frac{1}{35} \rho A_1 L (13 + 10\alpha) & -\frac{1}{420} \rho A_1 L^2 (22 + 15\alpha) \\ \text{Simetrik} & & & \frac{1}{840} \rho A_1 L^3 (8 + 5\alpha) \end{bmatrix} \quad (10)$$

where A_1 and ρ indicate the beam cross section area at the left and mass density, respectively. A_1 and α are given by.

$$\left. \begin{aligned} A_1 &= t_1 W \\ \alpha &= \frac{t_2 - t_1}{t_1} \end{aligned} \right\} \quad (11)$$

The Stiffness Matrix for the Crack

The amount of energy required for the elongation in front of the crack is called the strain energy release rate and indicated by J . For plane strain, J can be given as (Irwin, 1960):

$$J = \frac{1-\nu^2}{E} K_I^2 + \frac{1-\nu^2}{E} K_{II}^2 + \frac{1+\nu}{E} K_{III}^2 \quad (12)$$

where ν , E , K_I , K_{II} and K_{III} are Poisson's ratio, modulus of elasticity and the stress intensity factors for the mode I , II and III deformation types, respectively. Due to Castigliano's theorem and stress intensity factors, the flexibility coefficients that occur in the structure can be found. If U is the strain energy of a cracked structure with a crack area A under the load P_i , then the relation between J and U is

$$J = \frac{\partial U(P_i, A)}{\partial A}. \quad (13)$$

According to Castigliano's theorem, the additional displacement caused by the crack in the direction of P_i is as follows.

$$u_i = \frac{\partial U(P_i, A)}{\partial P_i} \quad (14)$$

If Eq. (13) is substituted into the Eq. (14), the following equation is obtained.

$$u_i = \frac{\partial}{\partial P_i} \int_A J(P_i, A) dA \quad (15)$$

Thus, the flexibility coefficients are as follows:

$$c_{ij} = \frac{\partial u_i}{\partial P_j} = \frac{\partial^2}{\partial P_i \partial P_j} \int_A J(P_i, A) dA \quad (16)$$

If it is assumed that the shear force does not affect the opening of the crack, the elastic coefficients for the displacement vector $\delta(u, v, \theta)$ can be written in matrix form as follows.

$$C = \begin{bmatrix} c_{11} & 0 & c_{13} \\ 0 & c_{22} & 0 \\ c_{31} & 0 & c_{33} \end{bmatrix}_{(3 \times 3)} \quad (17)$$

The inverse of the elasticity matrix will yield the stiffness matrix for a node point. The stiffness matrix is given as follows:

$$[C]^{-1} = \begin{bmatrix} \frac{c_{33}}{-c_{13}^2 + c_{11}c_{33}} & 0 & \frac{c_{13}}{c_{13}^2 - c_{11}c_{33}} \\ 0 & \frac{1}{c_{22}} & 0 \\ \frac{c_{13}}{c_{13}^2 - c_{11}c_{33}} & 0 & \frac{c_{11}}{-c_{13}^2 + c_{11}c_{33}} \end{bmatrix}_{3 \times 3} \quad (18)$$

For a beam with two nodes and three degrees of freedom at the each node, the stiffness matrix caused by the crack in the crack section is obtained as follows.

$$K_{cr} = \begin{bmatrix} [C]^{-1} & -[C]^{-1} \\ -[C]^{-1} & [C]^{-1} \end{bmatrix}_{(6 \times 6)} \quad (19)$$

where, K_{cr} is the stiffness matrix that occurs in the beam due to the crack.

Vibration Analysis of a Variable Cross-Section Cracked Beam

It is known that the crack in the structure causes a certain stiffness drop. Stiffness matrix for cracked beam $[K]_{wcr}$ can be found as follows.

$$[K]_{wcr} = [K] + [K]_{cr} \quad (20)$$

The equation for undamped free vibration of cracked beam can be given in matrix notation as (Haskul, 2010);

$$([K]_{wcr} - \lambda[M])\varphi = 0 \quad (21)$$

The λ values obtained from the solution of Eq. (21) will give the natural frequencies (ω^2) and the φ values will give the natural vectors of the cracked varying cross section beam.

NUMERICAL RESULTS

In this study, the natural frequency and mode shapes of the beam were obtained by conducting free vibration analysis of the beam with different boundary conditions with a single crack. The geometrical properties of the variable cross-section beam is; length $L=0.2$ m and t_1/t_2 varies linearly as shown in Figure 2. Calculation has been performed with the numerical values, Young's modulus $E = 216 \times 10^9$ Nm^{-2} , Poisson's ratio $\nu = 0.33$ and mass density $\rho = 7.85 \times 10^3$ kg m^{-3} .

Pinned-pinned cracked beam with constant width and variable thickness

As a first case, the free vibration analysis of a pinned-pinned cracked beam with constant width and variable thickness was analyzed and the natural frequencies and mode shapes of the beam were obtained.

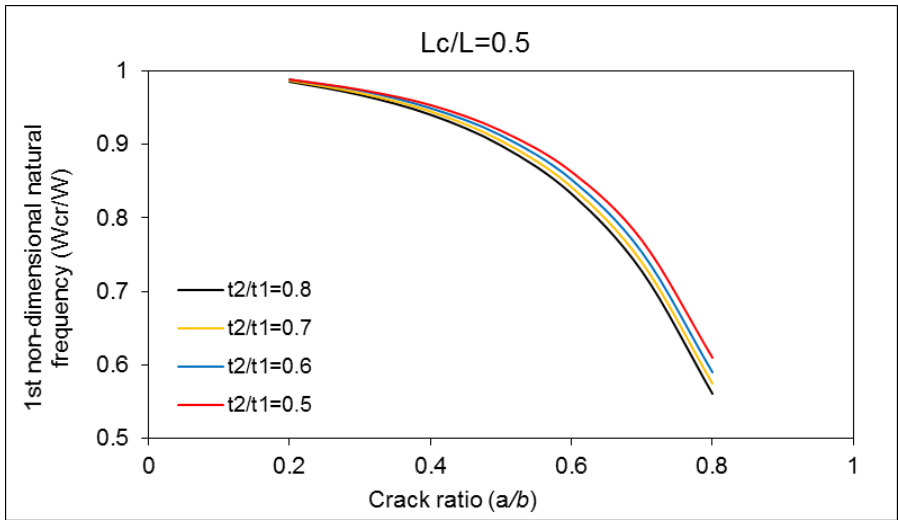


Figure 2. First non-dimensional natural frequencies of pinned-pinned cracked beam with varying cross section, depending on the crack location $L_c/L=0.5$, crack ratios and thickness ratios.

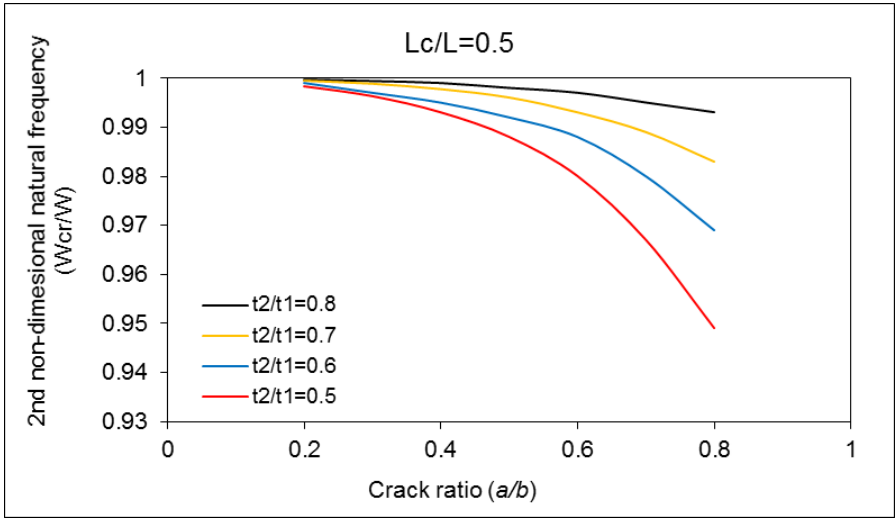


Figure 3. Second non-dimensional natural frequencies of pinned-pinned cracked beam with varying cross section, depending on the crack location $L_c/L=0.5$, crack ratios and thickness ratios.

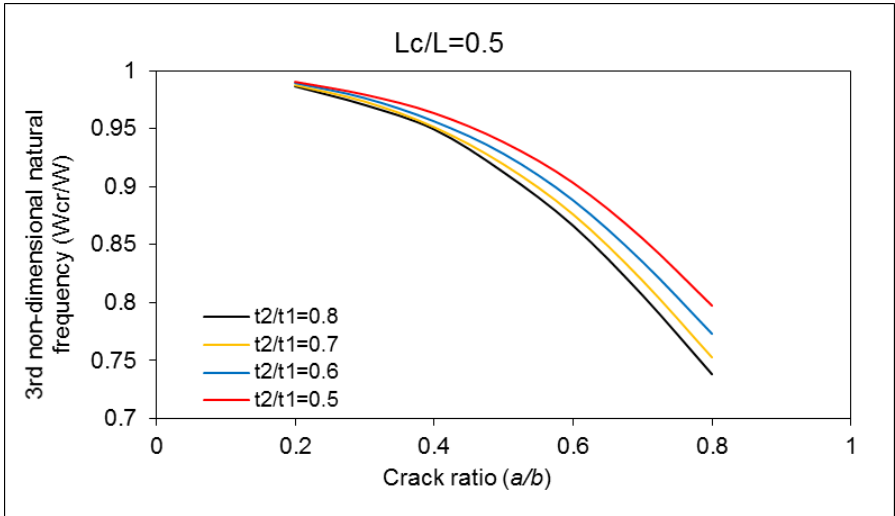


Figure 4. Third non-dimensional natural frequencies of pinned-pinned cracked beam with varying cross section, depending on the crack location $L_c/L=0.5$, crack ratios and thickness ratios.

Figures 2, 3, and 4 show the non-dimensional 1st, 2nd and 3rd natural frequencies according to the location of the crack $L_c/L = 0.5$, crack ratios $a/b=0.2, 0.4, 0.6, 0.8$ and thickness ratios $t_2/t_1=0.8, 0.7, 0.6, 0.5$ for the pinned-pinned cracked beam with constant width and variable thickness.

As can be seen from these figures, the biggest decrease occurred in the first natural frequency while the crack was in the middle ($L_c/L=0.5$). This is because the crack in this region causes maximum energy loss as the beam vibrates in the corresponding mode.

Accordingly, since the maximum bending moment in the vibrating beam in the first mode will occur in the middle, the crack in this region will cause the maximum energy loss and hence the maximum decrease will occur in the first natural frequency.

Again, as can be seen from the figures, the decrease in all natural frequencies (1st, 2nd and 3rd) increases as the crack (a/b) and thickness ratios (t_2/t_1) increase.

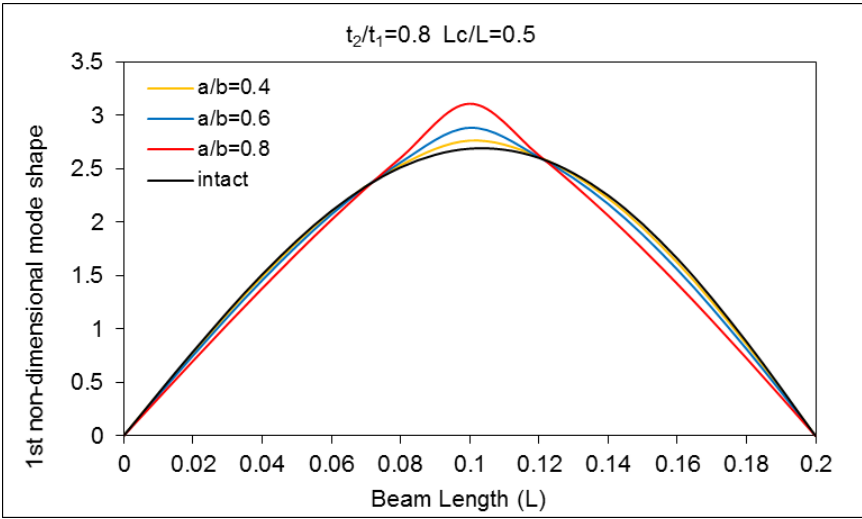


Figure 5. First non-dimensional mode shape of pinned-pinned cracked beam with varying cross section, depending on the crack location $L_c/L=0.5$, thickness ratio $t_2/t_1=0.8$ and crack ratios.

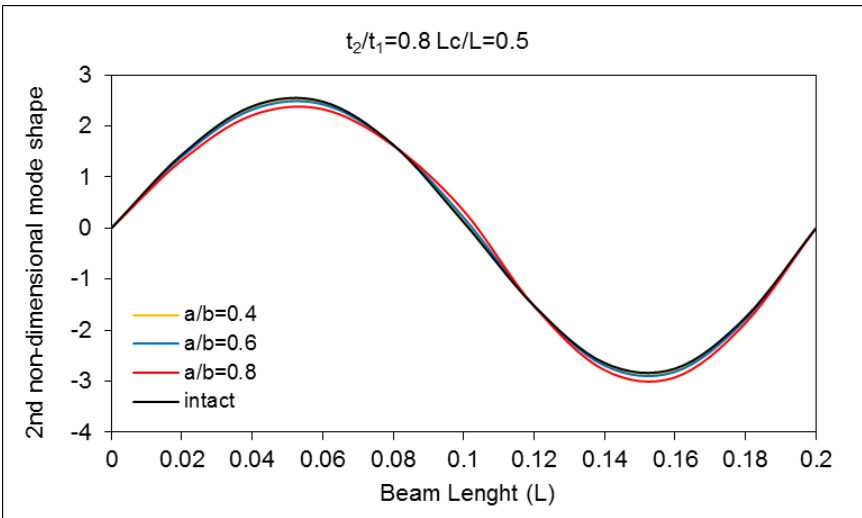


Figure 6. Second non-dimensional mode shape of pinned-pinned cracked beam with varying cross section, depending on the crack location $L_c/L=0.5$, thickness ratio $t_2/t_1=0.8$ and crack ratios.

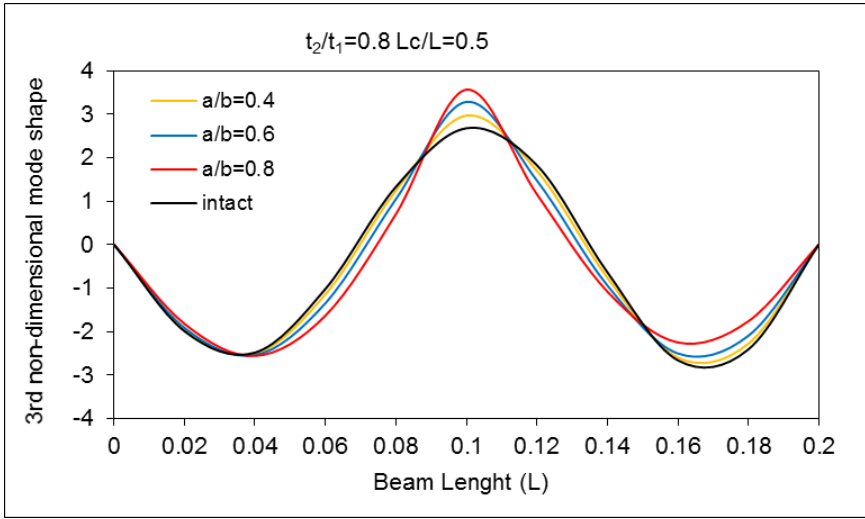


Figure 7. Third non-dimensional mode shape of pinned-pinned cracked beam with varying cross section, depending on the crack location $L_c/L=0.5$, thickness ratio $t_2/t_1=0.8$ and crack ratios.

Figures 5, 6, and 7 show the non-dimensional 1st, 2nd and 3rd mode shapes according to the location of the crack $L_c/L = 0.5$, thickness ratio $t_2/t_1=0.8$ and crack ratios $a/b=0.2, 0.4, 0.6, 0.8$ for the pinned-pinned non uniform cracked beam.

If the 1st, 2nd and 3rd natural mode vectors are compared to the natural vector of the intact beam; from these figures, it can be seen that the largest changes occur in the 1st, 3rd and 2nd natural mode vectors, respectively for the crack location $L_c/L=0.5$ and thickness ratio $t_2/t_1=0.8$.

The reason for these results is also because the crack in this region causes maximum energy loss as the beam vibrates in the corresponding mode.

It is evident from the figures that, the changes in the first three natural mode vectors (1st, 2nd and 3rd) increase as the crack ratio (a/b) gets higher.

Fixed-free cracked beam with constant width and variable thickness

Second case is the free vibration analysis of a fixed-free cracked beam with constant width and variable thickness. The natural frequencies and mode shapes of the beam were obtained by using the finite element method.

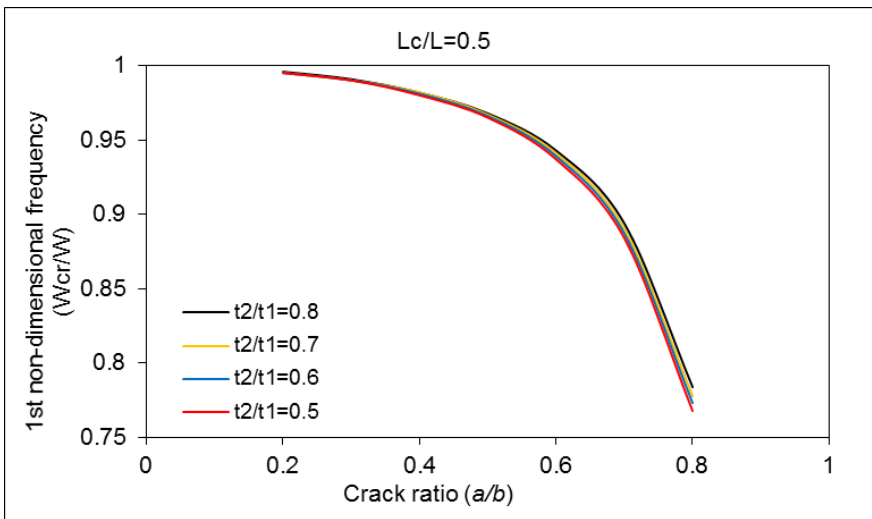


Figure 8. First non-dimensional natural frequencies of fixed-free cracked beam with varying cross section, depending on the crack location $L_c/L=0.5$, crack ratios and thickness ratios.

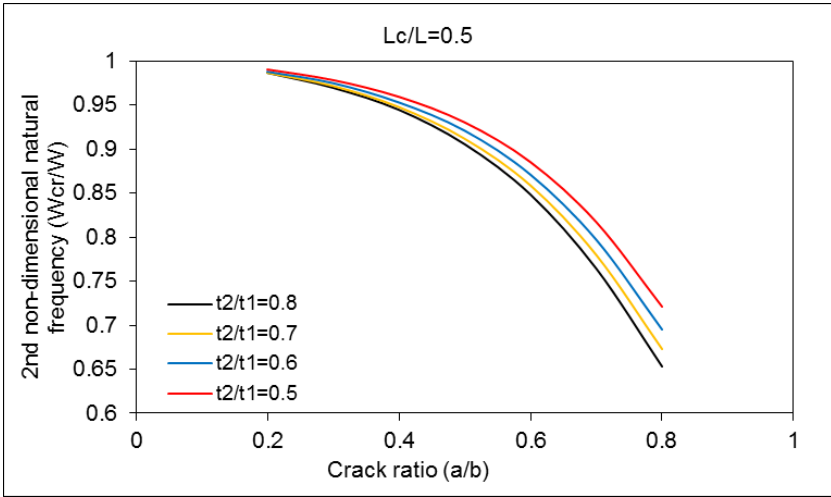


Figure 9. Second non-dimensional natural frequencies of fixed-free cracked beam with varying cross section, depending on the crack location $L_c/L=0.5$, crack ratios and thickness ratios.

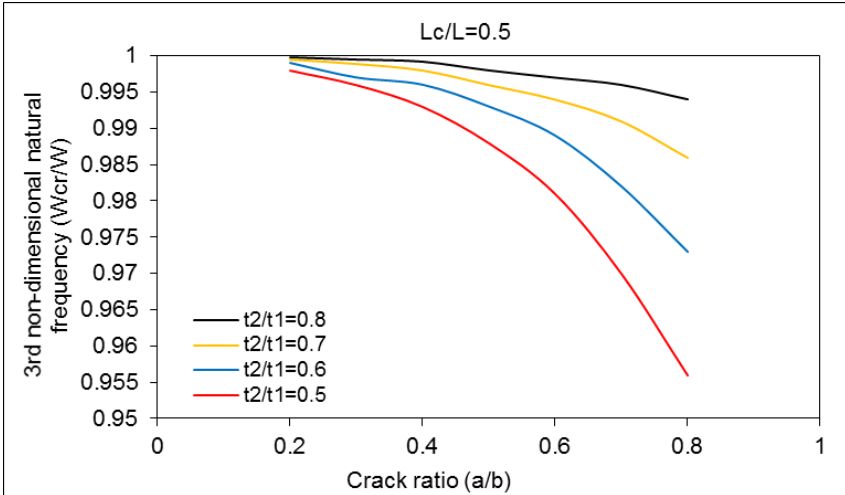


Figure 10. Third non-dimensional natural frequencies of fixed-free cracked beam with varying cross section, depending on the crack location $L_c/L=0.5$, crack ratios and thickness ratios.

Figures 8, 9, and 10 show the non-dimensional 1st, 2nd and 3rd natural frequencies according to the location of the crack $L_c/L = 0.5$, crack ratios $a/b=0.2, 0.4, 0.6, 0.8$ and thickness ratios $t_2/t_1=0.8, 0.7, 0.6, 0.5$ for the fixed-free cracked beam with constant width and variable thickness.

From these figures, it can be apparently seen that the biggest change occurs in 2nd, 1st and 3rd natural frequencies, respectively for the crack location $L_c/L=0.5$. The decrease in all natural frequencies (1st, 2nd and 3rd) rises as the crack (a/b) and thickness ratios (t_2/t_1) increase.

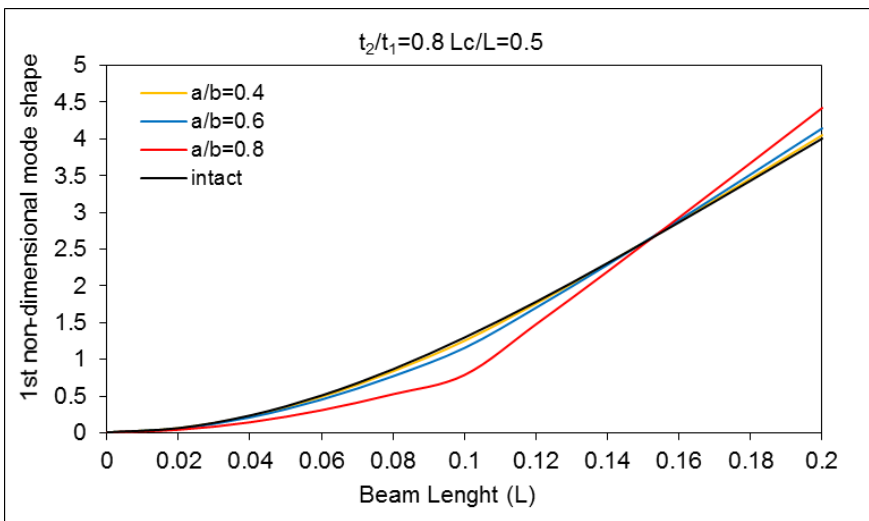


Figure 11. First non-dimensional mode shape of fixed-free cracked beam with varying cross section, depending on the crack location $L_c/L=0.5$, thickness ratio $t_2/t_1=0.8$ and crack ratios.

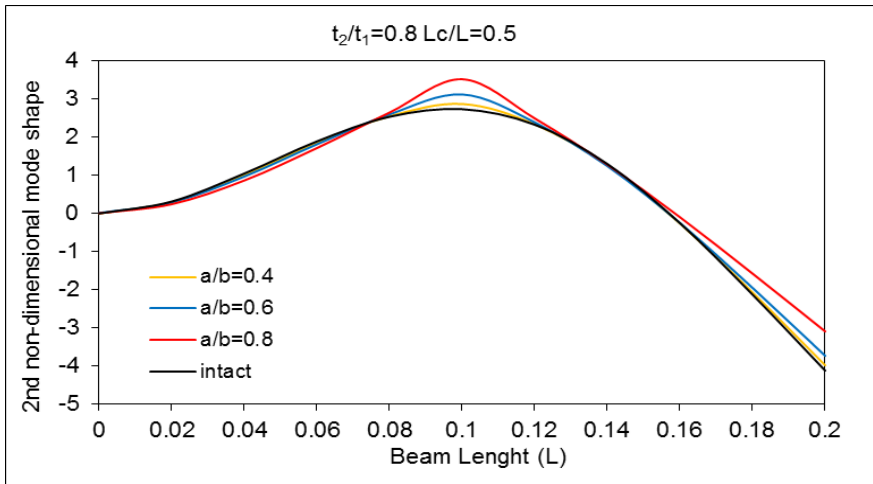


Figure 12. Second non-dimensional mode shape of fixed-free cracked beam with varying cross section, depending on the crack location $L_c/L=0.5$, thickness ratio $t_2/t_1=0.8$ and crack ratios.

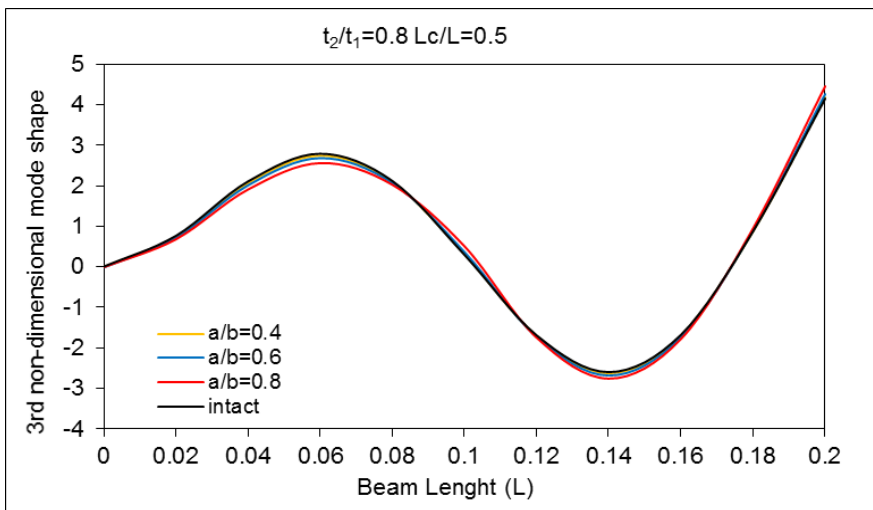


Figure 13. Third non-dimensional mode shape of fixed-free cracked beam with varying cross section, depending on the crack location $L_c/L=0.5$, thickness ratio $t_2/t_1=0.8$ and crack ratios.

Figures 11, 12 and 13 show the non-dimensional 1st, 2nd and 3rd mode shapes according to the location of the crack $L_c/L = 0.5$, thickness ratio $t_2/t_1=0.8$ and crack ratios $a/b=0.2, 0.4, 0.6, 0.8$ for the fixed-free non uniform cracked beam.

From the comparison of 1st, 2nd and 3rd natural mode vectors with that of intact beam; it can be seen that the largest change occurs in 2nd, 1st, 3rd natural mode vectors, respectively for the crack location $L_c/L=0.5$ and thickness ratio $t_2/t_1=0.8$.

The changes in the first three natural mode vectors (1st, 2nd and 3rd) increase as the crack ratio (a/b) rises.

CONCLUSION

Free vibration analysis of the cracked beam has been performed by using the finite element method. The beam was assumed to have constant width, variable thickness and a single non propagating edge crack. The free vibration analysis of non-uniform cracked beam having two different boundary conditions (pinned-pinned, fixed-free) was carried out.

The effects of thickness ratios, location of crack and crack depth ratios on the vibration parameters were investigated and illustrated in figures. While a crack in the middle of the pinned-pinned beam results in biggest decrease in the first natural frequency, the same crack causes most decrease in the second natural frequency in the fixed-free beam.

The reason for these results is the moment distribution in vibration modes. A crack in the cross section with a large bending moment will cause a significant amount of energy drop, which will change the vibration characteristics.

For the both cases it was shown that, the changes in the first three natural frequencies (1st, 2nd and 3rd) increase as the crack ratio (a/b) gets higher. The similar results have been found for the mode shapes of cracked beam with variable cross section.

REFERENCES

- Amirikian, A. (1951). Wedge-beam framing. In *Proceedings of the American Society of Civil Engineers* (Vol. 77, No. 1, pp. 1-36). ASCE.
- Avakian, A., & Beskos, D. E. (1976). Use of dynamic stiffness influence coefficients in vibrations of non-uniform beams. *Journal of Sound Vibration*, 47, 292-295.
- Al-Gahtani, H. J., & Khan, M. S. (1998). Exact analysis of nonprismatic beams. *Journal of engineering mechanics*, 124(11), 1290-1293.
- Bayat, M., Pakar, I., & Bayat, M. (2011). Analytical study on the vibration frequencies of tapered beams. *Latin American Journal of Solids and Structures*, 8(2), 149-162.
- Friedman, Z., & Kosmatka, J. B. (1992). Exact stiffness matrix of a nonuniform beam—i. extension, torsion, and bending of a bernoulli-euler beam. *Computers & structures*, 42(5), 671-682.
- Franciosi, C., & Mecca, M. (1998). Some finite elements for the static analysis of beams with varying cross section. *Computers & structures*, 69(2), 191-196.
- Gaines, J. H., & Volterra, E. (1966). Transverse vibrations of cantilever bars of variable cross section. *the journal of the Acoustical Society of America*, 39(4), 674-679.
- Gaines, J. H., & Volterra, E. (1968). Upper and Lower Frequencies Tapered Beams. *Journal of the Engineering Mechanics Division*, 94(2), 265-488.
- Ghali, A. and Neville, A. M., 1972. *Structural Analysis*, Intext Educ, Publ, Scranton, penn

- Haskul, M., 2010. Çatlak İçeren Değişken Kesitli Kirişlerde Titreşim Probleminin Sonlu Elemanlar Metoduyla Modellenmesi. Şanlıurfa, Türkiye.
- Irwin, G., (1960). Fracture Mechanics, Editors J. N. Goodier and N. J. Hoff, Pergamon Pres, New York. 368p.
- Just, D. J. (1975). Analysis of plane frames of linearly varying rectangular section. *The Structural Engineer*, 53, 12-16.
- Just, D. J. (1977). Plane frameworks of tapering box and I-section. *Journal of the Structural Division*, 103(1), 71-86.
- Karabalis, D. L., & Beskos, D. E. (1983). Static, dynamic and stability analysis of structures composed of tapered beams. *Computers & Structures*, 16(6), 731-748.
- Klein, L. (1974). Transverse vibrations of non-uniform beams. *Journal of Sound and Vibration*, 37(4), 491-505.
- Koloušek, V., & McLean, R. F. (1973). Dynamics in engineering structures. Butterworths.
- Li, Q. S. (2002). Free vibration analysis of non-uniform beams with an arbitrary number of cracks and concentrated masses. *Journal of Sound and Vibration*, 252(3), 509-525.
- Martin, H. C. (1966). Introduction to matrix methods of structural analysis (Book on matrix methods of structural analysis including truss, beams, coordinate transformations, force and displacement methods, programming, etc). *NEW YORK, MCGRAW-HILL BOOK CO., 1966. 331 P.*
- Martin, A. I. (1956). Some integrals relating to the vibration of a cantilever beam and approximation for the effect of taper on

- overtone frequencies. *The Aeronautical Quarterly*, 7(2), 109-124.
- Mazanoglu, K., & Sabuncu, M. (2010). Vibration analysis of non-uniform beams having multiple edge cracks along the beam's height. *International Journal of Mechanical Sciences*, 52(3), 515-522.
- Newmark, N. M. (1943). Numerical procedure for computing deflections, moments, and buckling loads. *Transactions of the American Society of Civil Engineers*, 108(1), 1161-1188.
- Rissone, R. F., & Williams, J. J. (1965). Vibrations of non-uniform cantilever beams (Finite difference method for analyzing vibrations of continuous variable-section cantilever turbine blades). *The Engineer*, 220, 497-506.
- Ruta, P. (2002). Dynamic stability problem of a non-prismatic rod. *Journal of sound and vibration*, 250(3), 445-464.
- Tan, G., Liu, Y., Gong, Y., Shen, Y., & Liu, Z. (2018). Free Vibration of the Cracked Non-uniform Beam with Cross Section Varying as Polynomial Functions. *KSCE Journal of Civil Engineering*, 22(11), 4530-4546.
- Thomas, J., & Dokumaci, E. (1973). Improved finite elements for vibration analysis of tapered beams. *The Aeronautical Quarterly*, 24(1), 39-46.
- Takahashi, I. (1999). Vibration and stability of non-uniform cracked Timoshenko beam subjected to follower force. *Computers & structures*, 71(5), 585-591.

Zheng, D. Y., & Fan, S. C. (2001). Natural frequencies of a non-uniform beam with multiple cracks via modified Fourier series. *Journal of Sound and Vibration*, 242(4), 701-717.

CHAPTER 4

**DETERMINATION OF AMOUNTS OF As, Cr, Pb and
Mn ELEMENTS IN MOLASSES PRODUCED FROM
CAROB: COMPARISON OF TRADITIONAL AND
INDUSTRIAL PRODUCTION**

Lecturer Dr. Hacer Sibel KARAPINAR¹

Prof. Fevzi KILICEL²

¹ *Scientific and Technological Research & Application Center, Karamanoğlu Mehmetbey University, 70200, Karaman, Turkey, sibelkarapinar@kmu.edu.tr*

² *Department of Chemistry, Karamanoğlu Mehmetbey University, 70200, Karaman, Turkey, fevzi@kmu.edu.tr*

1. INTRODUCTION

Molasses is a sweet and delicious product that can be prolonged with the shelf life produced by concentrating sugar-rich fruit juices by boiling without adding sugar and other additives. It is a traditional food produced from fruits such as grapes, mulberries, figs, plums, apricots, apples and carobs in almost every region of our country for many years. Generally breakfast is mixed with plain or tahini and can be consumed instead of jam or honey, but it is also used in the production of some local dishes. Molasses is a food rich in carbohydrates, organic acids, mineral substances and partly vitamins. It is important in terms of nutrition because of the sugar it contains (Şimşek and Artık, 2002). 100% of total sugars in grape molasses and 80% in other molasses varieties consist of monosaccharides such as glucose and fructose (Sengül et al., 2007). Heavy metals are substances that have a relatively high density and are toxic or toxic even at low concentrations. Heavy metals are a collection of more than 60 metals, including lead (Pb), cadmium (Cd), iron (Fe), cobalt (Co), copper (Cu), nickel (Ni), mercury (Hg) and zinc (Zn) (Kahvecioğlu et al., 2003). It is stated that the most toxic effects of heavy metals are Cd, Pb and Hg (Çepel, 1997). The carob tree (*Ceratonia siliqua* L.) is of major socio-economic benefits to rural development and mountain economy. The carob fruit is technically 15-30 centimeters long and has a very thick and broad legume (Sidina et al., 2009). In this study, it was aimed to determine the heavy metal levels in carob molasses collected from the villages and markets of

Karaman and to emphasize the importance of nutrition in carob molasses.

2. MATERIALS and METHODS

2 samples of homemade (traditional production) and 2 samples of market (industrial production) carob molasses were used in this study

The sample preparation: The samples were prepared to be 2 parallel for each sample and were solutioned by wet burning method. For this purpose, from the collected samples, weighed 2 g with precision scales and placed in 100 ml beakers and 16 ml of HNO_3 (65%, w/w) were added. 4 ml HClO_4 (70-72%, w/w) are added to it and the solution is slowly heated in the drawer for about 5-6 hours. The heating process close to the end of the acids is cut off and the solutions are cooled. Then 5 ml H_2O_2 (30%, w/w) was added and heating was continued until clear liquid was obtained. Heating was stopped when clear liquid was formed, and the solutions were allowed to cool. Cooling solutions were filtered through blue band filter paper and 20 ml of the obtained solutions were mixed with distilled water to prepare the analyzed. The concentrations of the determined elements were determined by Inductively Coupled Plasma Optical Emission Spectrometry.

The preparation of standard solutions: Definite-concentration certificated standards have been used. 1000 ppm standards have been used as main stock. From main stock solution as study standards; it has been prepared in HNO_3 setting of 2 M 65% and as to be 100 ml.

3. RESULTS

The amounts of elements in molasses are given in Table 1 and Figure 1, 2, 3.

Table 1. Element amounts in molasses (mg/kg)

		Sample				
		No	As	Cr	Mn	
					Pb	
Industrially produced molasses (A brand)	1	1.68	0.047	2.549	0.655	
	2	1.754	-	2.571	0.806	
	3	2.067	0.048	2.546	0.520	
	4	1.750	0.068	2.720	0.603	
	5	1.938	0.033	2.705	0.898	
	6	1.825	0.025	2.698	0.516	
			1.836±0.143	0.044±0.016	2.632±0.084	0.666±0.156
Industrially produced molasses (B brand)	1	-	-	0.202	-	
	2	-	-	0.196	-	
	3	-	-	0.193	-	
	4	-	-	0.338	-	
	5	-	-	0.328	-	
	6	-	-	0.314	-	
			0.262±0.072			
Traditional produced molasses (A village)	1	-	-	0.379	-	
	2	-	-	0.360	-	
	3	-	-	0.393	-	
	4	-	-	0.240	-	
	5	-	-	0.249	-	
	6	-	-	0.239	-	
			0.310±0.075			
Traditional produced molasses (B village)	1	-	-	5.003	-	
	2	-	-	4.938	-	
	3	-	-	5.051	-	
	4	-	-	4.528	-	
	5	-	-	4.492	-	
	6	-	-	4.026	-	
			4.673±0.399			

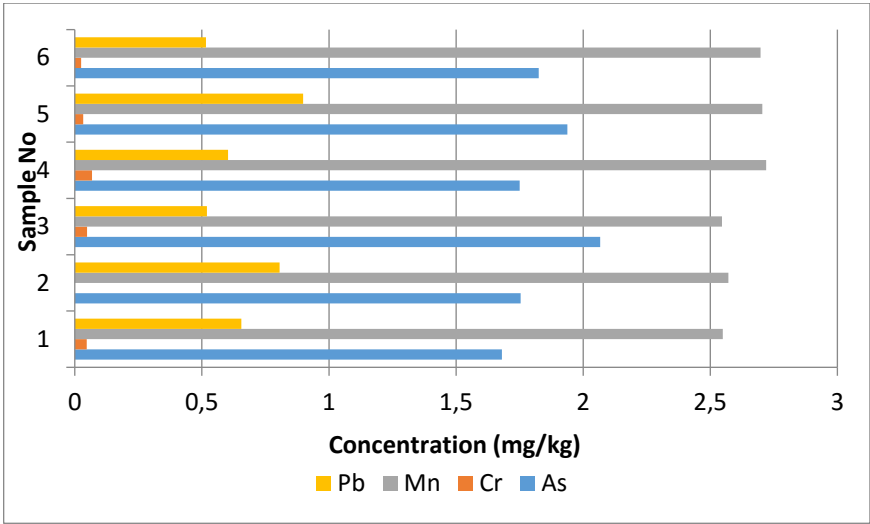


Figure 1. Industrially produced molasses (A brand)

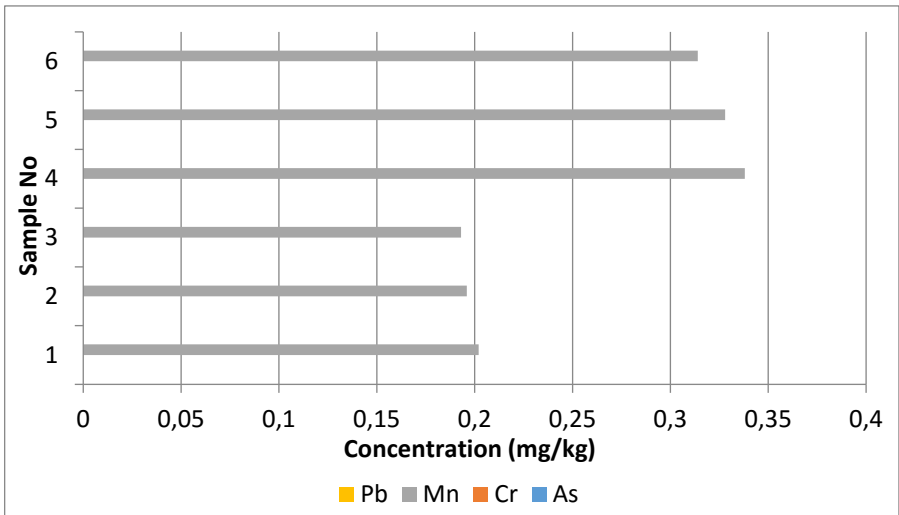


Figure 2. Industrially produced molasses (B brand)

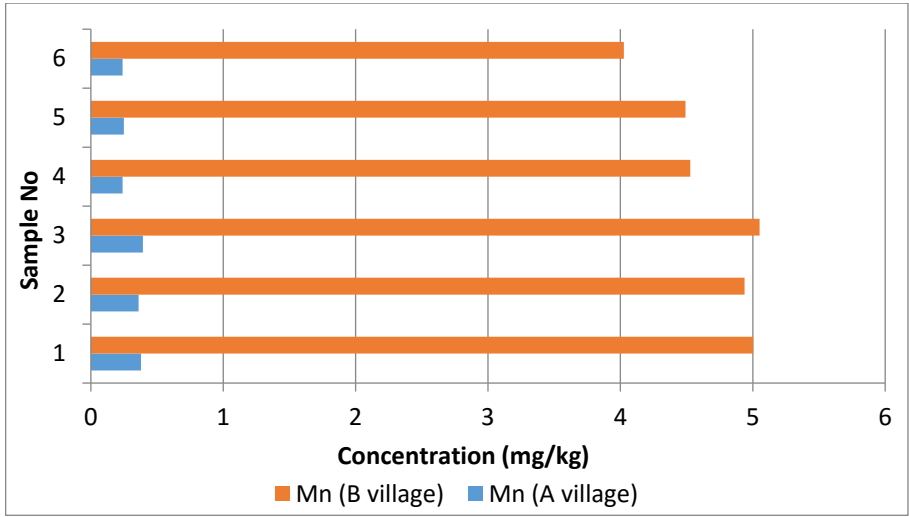


Figure 3. Traditional produced molasses

4. DISCUSSION

According to the results, As, Cr, Pb and Mn elements of A brand molasses were determined. Only the Mn element was identified in the B brand molasses and the traditionally produced molasses.

The World Health Organization (WHO), Food and Agriculture Organization (FAO), The Turkish Food Codex (TFC) according to the values of the elements of the table is given in Table 2.

Table 2. Evaluation of quantities of elements (WHO, 1999; WHO, 2007; Anonim, 2017)

	Element	Founded value	Acceptable value	Evaluation
WHO, FAO	Pb	0.516 -0.898	10.0	Low
	Mn	0.193-5.051	2.0 – 9.0	Normal
TFC	Pb	0.516 -0.898	0.3	High

It is important to inform our people about molasses consumption because molasses is a very important food for nutrition. According to the results, it was seen that the molasses produced by traditional means were healthier.

5. REFERENCES

- Anonymous, 2017, Turkish Food Codex Communiqué on Grape Molasses, Turkish Food Codex, <http://www.mevzuat.gov.tr/Metin.Aspix> (Accessed on: 01.12.2017).
- Çepel, N. (1997). Soil Pollution Erosion and Environmental Damage. Turkey Combating Soil Erosion, forestation and Natural Heritage Protection Foundation Press, (14).
- Kahvecioğlu, Ö., Kartal, G., Güven, A., & Timur, S. (2003). Environmental effects of metals-I. *Metallurgical Journal*, 136, 47-53.
- Sengül, M., Fatih Ertugay, M., Sengül, M., & Yüksel, Y. (2007). Rheological characteristics of carob pekmez. *International Journal of Food Properties*, 10(1), 39-46.
- Sidina, M. M., El Hansali, M., Wahid, N., Ouattmane, A., Boulli, A., & Haddioui, A. (2009). Fruit and seed diversity of domesticated carob (*Ceratonia siliqua* L.) in Morocco. *Scientia horticultrae*, 123(1), 110-116.
- Şimşek, A., Artık, N., & Baspınar, E. (2004). Detection of raisin concentrate (Pekmez) adulteration by regression analysis method. *Journal of Food Composition and Analysis*, 17(2), 155-163.
- World Health Organization., 1999. WHO Monographs on Selected Medicinal Plants, Vol. I, Geneva, Switzerland. 1-295.
- World Health Organization., 2007. WHO Guidelines for Assessing Quality of Herbal Medicines with Reference to Contaminants and Residues. Spain. 1-105.

CHAPTER 5
WA-XRD ANALYZES OF DIFFERENT KINDS OF
COMPOSITE FILLING MATERIALS

Assist. Prof. Tülay GÜRSOY¹

¹ Van Yuzuncu Yil University, Faculty of Science, Department of Chemistry. Van, Turkey. tulaygursoy@yyu.edu.tr

INTRODUCTION

Almost all of the composite filling materials form the polyurethane compound. Polyurethanes are common high molecular components used as a raw materials for a large number of modern polymeric materials (Cinelli et al., 2013).

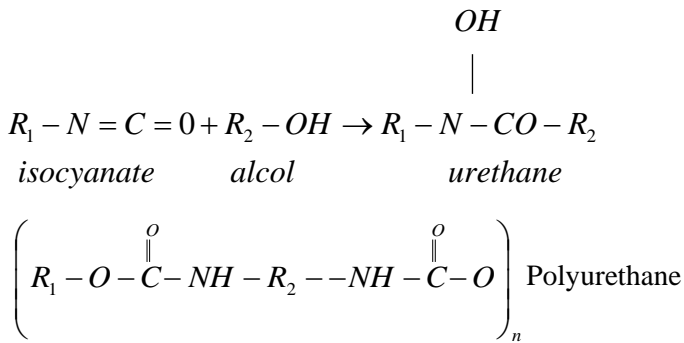


Figure 1. Polyurethane formation reaction (Aydın and Ekmekçi, 2002).

Polyurethane application areas are as follows:

Construction Sector	: %26.8	Textil Sector	: %3.3
Transport Sector	: %23.8	Machine Sector	: %3.3
Furniture Sector	: %20.7	Electronic Sector	: %1.4
Inst. and Device Sector:	%5.1	Shoe and Slipper Sector	: %0.7
Packing Sector	: %4.6	Other Sectors	: %10.2

More than 75% of the worldwide consumption of polyurethanes, which have a wide usage area, is in the form of foam. Polyurethane foam is frequently used in thermal insulation, sound insulation,

industrial jacketing and packaging materials (Anonymous, 2014; 2017).

Polyurethane foams production techniques;

1. Block Casting
2. Sheet Casting
3. Spraying
4. Pouring
5. Double Tape Rolling
6. Moulding

can be listed as (Aydın and Ekmekçi, 2002).

The main raw materials of polyurethane foams are polyol (polyether and polyester) and isocyanate. The general, the rate of exothermic polymerization reaction in which the room temperature is sufficient can be controlled using catalyst. The structural properties of polyurethane foams can be adjusted by the type and amount of the polyol/isocyanate (OH/NCO) ratio, flame retardant, surfactant and blowing agents. Since polyols (polyether and polyester) and isocyanate chemicals are from petroleum residues, their raw materials are exhausted every day. In addition, it is not renewable and biodegradable, increases the amount of CO₂ and accelerates global warming (Pan et al., 2011). For this reason, polyurethane based foams are made of different lignocellulosic materials which are abundant in both nature and agricultural production areas.

The preparation of low-cost polyols from abundant and renewable biomass sources has long been an area of interest in the polyurethane industry (Yao et al., 1996). Many scientific efforts to achieve biomass utilization and greater use of biomass include starch, cellulose powders, lignocellulosic materials, lignin and the like plant components to be incorporated into polyurethane foams (Hostettler, F., 1979; Hatakeyama et al., 1992). Liquefaction of biomass to produce industrial chemicals is a method for using biomass sources. Researches on this began with the liquefaction of wood meal (Besteu et al., 1965; Maldas and Shiraishi, 1997; Vuori and Niemela, 1998; Yamada and Ono, 1999). In contrast, the reaction conditions were difficult to use in practice and consumed a lot of energy. Researchers facilitated reaction conditions and used liquefied product to produce resin and foam (Alma et al., 2003; Lin et al., 1994).

The principles and methods of liquefaction of wood meal have given some ideas for the use of agricultural wastes with similar composition as wood meal (Wang and Chen, 2007). Some studies have been carried out on liquefaction of agricultural wastes (Cinelli et al., 2013; Wang and Chen, 2007; Alma et al., 2003; Lin et al., 1994; Yao et al., 1993; Wang et al., 2013; Hakim et al., 2011).

The insertion of biomass materials into the polyurethane systems is by difficult steps that increase the biomass content; affects the chain stiffness, durability, chain length, density and thermal properties of polyurethane foams (Ferrigno, 1967; Hsu and Glasser, 1976).

Two different approaches are being used to produce bi-material in the production of polyurethane materials. The first is includes starch,

lignocelluloses, coffee, etc direct joining of biomass (Hostettler, 1979; Kohn and Rober, 1988; Yoshida et al., 1987). The second is the use of biomass by the hydroxylation reaction (Hakim et al., 2011, Barikani and Mohammadi, 2006). Biomass-containing polyurethane foam is produced by mixing a certain amount of liquefied biomass, catalyst, surfactant and foaming agent in a container and than by mixing the mixture with a certain amount isocyanate and stirring it rapidly (Wang et al., 2013; Alma et al., 2002).

MATERIALS AND METHODS

The wastes of potato, pistachio and barley were dried under atmospheric pressure. Waste meals (0-80 mesh) were dried in an oven at $103 \pm 2^{\circ}\text{C}$ for 24 hours before re-use. The liquefaction reagent was a mixture of PEG#400 and glycerin with a mass ratio of 4/1 (w/w). Sulfuric acid was used as catalysts and liquefaction reactions of biomass were realized by microwave heating method. The normal heating program was used, which was at 350 watt/min with 300 rpm/min mixing speed (**1st step polymerization reaction**). Liquefied and non-liquefied plant components were dissolved with 200 mL of methanol and isolated with the aid of an aqueous type vacuum pump (TVP 200).



Potato crust



Potato crust mill



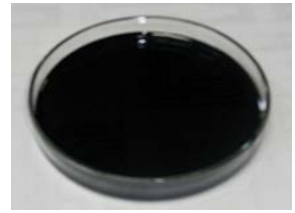
Liquefaction reagents



Liquefaction react.



Unliquefied parts



Liquefied potato

Figure 2. Photographs of potato crust, potato crust miles, liquefaction reagents, liquefaction reaction, unliquefied parts, liquefied potato crust.



Pistachio red peel



Pistachio stiff peel



Red peel miles



Stiff peel miles



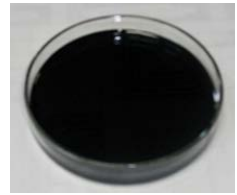
Liq. reagents



Liq. reaction



Unliquefied red peel



Liquefied red + stiff peel

Figure 3. Photographs of pistachio red peel, pistachio stiff peel, pistachio waste miles, liquefaction reagents, liquefaction reaction, liquefied pistachio peels, unliquefied parts.



Barley Straw



Barley Straw Miles



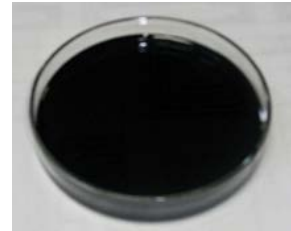
Liquefaction
Reactives



Liquefaction reaction



Unliquefied Parts



Liquefied Barley
Straw

Figure 4. Photographs of barley straw, barley straw miles, liquefaction reagents, liquefaction reaction, unliquefied parts, liquefied barley straw.

Preparation of the Rigid Foams

The definite amounts of liquefied plant polyols, polyetilen glikol 400, catalyst, surfactant and water premixed thoroughly in a plastic cup. Then, the prescript amount of MDI (at an isocyanate index of 90) was added and mixed quickly at a high stirring speed of 8.000 rpm for 15-20 seconds (**2nd step polymerization reaction**). It was allowed to rise freely at room conditions. Foams were allowed to cure at room temperature for two days and then were removed from the plastic cup before cutting into test samples.

WA-XRD Analysis (Wide-angle X-ray Diffraction)

Wide-angle X-ray diffractometer analysis were performed to investigate the polymer structure of polyurethane foams derived from plant's wastes and commercial synthetic one at molecular level. Another aim is to examine the changes in the crystal structure of the plant's waste components. In addition to above, wide-angle X-ray diffraction was used to study the interplaner distances (d-spacing) in the PU crystal-line samples. The d-spacings corresponding to the large peaks in the respective curves were calculated from Bragg's equation:

$\lambda = 2 (d\text{-spacing}) \sin \phi$ where 2ϕ is the X-ray scattering angle.

Sheets were measured with wide-angle X-ray diffraction (WAXRD) (Philips X' Pert PRO mark XRD (reflection) machine). For irradiation, the $\text{CuK}\alpha$ line was applied (λ at 0,154056 nm, cathode at 40 kV and 30 mA) and scattering was recorded in the range of $2\phi=10\text{-}70^\circ$.

FINDINGS

Table 1. Effects of the reaction conditions on liquefaction reaction of potato crust.

Biomass	Sulphuric acid catalyst concentration	Reaction time (min)	PDIP (%)	Reaction Completion Temperature (°C)
Potato crust	9	15	4.48	85.3
Potato crust	4	15	6.04	83.2
Potato crust	3	15	9.25	81.2
Potato crust	9	30	0.60	102.0
Potato crust	4	30	4.70	95.4
Potato crust	3	30	5.74	89.2

Conditions: Potato crust/PEG400/Glycerin = 5/12/3, 350 watt/min microwave-heating energy, 300 rpm/min mixing speed

^a PDIP: Percent dissoluble Part (%)

Table 2. Effects of the reaction conditions on liquefaction reaction of pistachio peels.

Biomass	Sulphuric acid catalyst concentration	Reaction time (min)	PDIP (%)	Reaction Completion Temperature (°C)
Pistachio peel	6	15	11.85	101.7
Pistachio peel	9	15	09.95	98.30
Pistachio peel	12	15	11.85	95.30
Pistachio peel	15	15	12.35	94.50
Pistachio peel	6	30	17.20	103.0
Pistachio peel	9	30	21.35	102.0
Pistachio peel	12	30	31.65	100.0
Pistachio peel	15	30	42.55	88.80

Conditions: Pistachio peel/PEG400/Glycerin = 5/12/3, 350 watt/min microwave-heating energy, 300 rpm/min mixing speed

^a PDIP: Percent dissoluble Part (%)

Table 3. Effects of the reaction conditions on liquefaction reaction of barley straw.

Biomass	Sulphuric acid catalyst concentration	Reaction time (min)	PDIP (%)	Reaction Completion Temperature (°C)
Barley straw	12	10	17.60	102.1
Barley straw	12	20	20.70	103.2
Barley straw	12	30	19.40	88.60
Barley straw	15	10	11.59	123.0
Barley straw	15	20	14.70	95.40
Barley straw	15	30	13.00	89.20

Conditions: Barley Straw/PEG400/Glycerin = 2.5/12/3, 350 watt/min microwave-heating energy, 300 rpm/min mixing speed

^a PDIP: Percent dissoluble Part (%)

Table 4. Foam formulations for the liquefied potato waste-based polyols.

Ingredients	Parts by Weight
Potato crust-based polyol	100
Catalyst	3
1. Surfactant	2.5
Liq. Blowing agent (water, including water from neutralization with NaOH solution)	6.25
PEG 400	20
2. MDI	130
Liq. pH	6.85

Table 5. Foam formulations for the liquefied pistachio waste-based polyols.

	Ingredients	Parts by Weight
	Pistachio peel-based polyol	100
	Catalyst	3.5
	Surfactant	2.8
1. Liq.	Blowing agent (water, including water from neutralization with NaOH solution)	1.0
	PEG 400	20
2. Liq.	MDI	150
	pH	6.5

Table 6. Foam formulations for the liquefied barley waste-based polyols.

	Ingredients	Parts by Weight
	Barley crust-based polyol	100
	Catalyst	6
1. Liq.	Surfactant	5
	Blowing agent (water, including water from neutralization with NaOH solution)	12.5
	PEG 400	40
2. Liq.	MDI	260
	pH	7.56

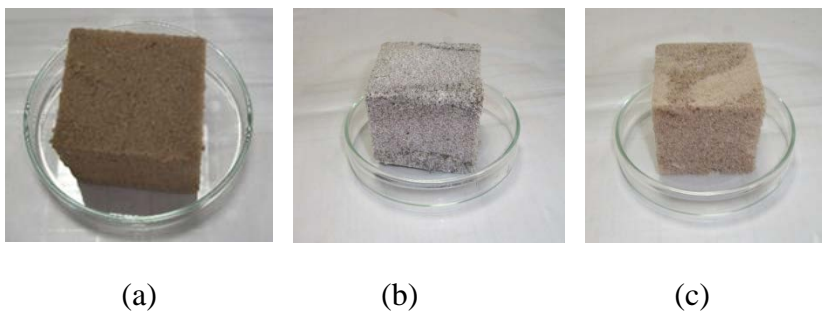


Figure 5. (a) Potato waste-foam, (b) pistachio waste-foam, (c) barley waste-foam

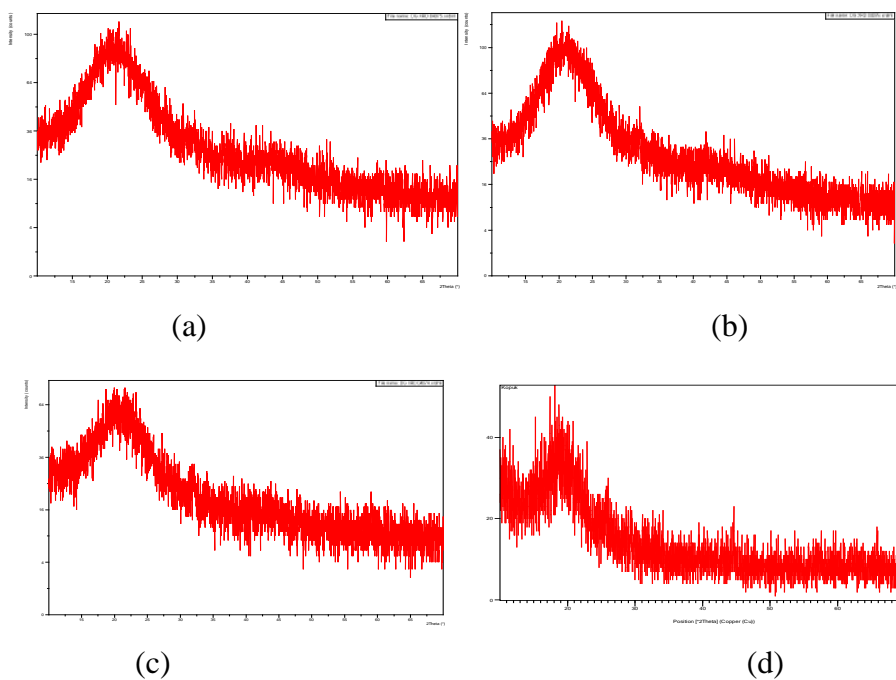


Figure 6. WA-XRD patterns of (a) Potato waste foam, (b) Pistachio waste foam, (c) Barley-waste foam, (d) commercial synthetic foam

WA-XRD analysis of potato waste foam

From the WA X-ray diffraction pattern, the PU foam derived from the potato wastes appears unique and amorphous structure and correspondingly has superior mechanical properties. The atomic structure is irregular but compatible with the polymer structure. The PU foam derived from potato waste has a WA X-ray diffraction peak between 13.1° - 28.5° . The sharp, high diffractom of the potato crust starch, which is close to 20.6° in 2θ value is the agglomeration area of the small amount of starch, and the diffraction peak of the potato crust cellulose, which is close to 19.4° , in 2θ value indicates the agglomeration area of the small amount of cellulose. However, for both crust starch and cellulose, the density of these peaks is reduced or lost. This is a sign that the bond between the potato crust and the polyurethane pre-polymer changes the basic crystal form of the potato crust (Zou et al., 2011; Savelyev et al., 2014; Zhang et al., 2012).

WA-XRD analysis of pistachio waste foam

From the WA X-ray diffraction pattern, the PU foam derived from the pistachio peels is unique and amorphous structure, and the atomic structure is irregular but compatible with the polymer structure. Pistachio peel-contained PU foam has a WA X-ray diffraction pike in the range of 14.9 - 27.6° . The sharp, high diffractom of pistachio peel cellulose, which is close to 20.6° in 2θ indicates the agglomeration area of the small amount of cellulose (Wang et al., 2013; Gang et al., 2017).

WA-XRD analysis of barley waste foam

From the WA X-ray diffraction pattern, the PU foam derived from the barley straw is unique and amorphous and has a WA X-ray diffraction pike in the range of 13.9-26.3°. The sharp and high diffractom of barley straw lignin, which is close to 20.1° in 2θ indicates the agglomeration area of the small amount of lignin (Wang et al., 2013; Gang et al., 2017).

WA-XRD analysis of commercial synthetic foam

Syntetic PU foams showed a diffuse peak located at 18.5° of 2θ , in spite of the fact that -C=O- based hydrogen bonds constructed a small scale ordered domain in the PU matrix. In this case, -NH in the hard segment was hydrogen bonded with the -C=O of the hard segments and the ester -C=O of the glycerin soft segments (Wang et al., 2010; Zou et al. 2011). From total diffractogram, it can be seen that the synthetic foam has also a unique and amorphous structure and a wide-angle X-ray diffraction pike in the range of 12.5-23.8°.

CONCLUSIONS

• Composite PU foams which contains 25% potato wastes polyol (w/w), 25% pistachio wastes polyol(w/w) and 12.5% barley wastes polyol (w/w) synthesized.

• All four types of composite materials which analyzed of WA-XRD are amorphous structure.

• X-ray diffraction peak angles are different.

• A linear ratio was determined between the increased amount of biomass corroded to the structure and the amorphous property and X-ray diffraction peak angle range (Trovati et al., 2010).

• When the Bragg's equation evaluated, the diffraction peaks decreased.

• The degree of crystallinity reduced by the addition of biomass according to potato waste foam> pistachio waste foam> barley waste foam> synthetic foam sequence (Wei et al., 2000; Yasushi et al., 1972).

• According to the energy experts, the energy demand in the 2030s will be 60% more than today. Considering the share of energy consumption, the importance of composite filling materials is increasing day by day (Bayülken and Kütükoğlu, 2009).

REFERENCES

- Alma, M. H., Bařtırık, M. A., Dıđrak, M., 2002. Liquefaction of agricultural biomass wastes with polyhydric alcohols and its application to polyurethane-type foams. *12 th European Conference on Biomass for Energy, Industry and Climate Protection*, 17-22 Haziran 2002, Amsterdam, 1247-1250.
- Alma, M. H., Bařtırık, M. A., Dıđrak, M., 2003. New polyurethane-type rigid foams from liquefied wood powders. *Journal of Materials Science Letter*, 22: 1225-1228.
- Anonymous, 2014. Poliüretanların Kullanım Alanları. <http://www.putechmagazine.com/Haber/Poliuretan-Kimyası-Son-Gelismeler.html>. Putech Kompozitez Poliüretan ve Kompozit Sanayi Dergisi, İstanbul. Eriřim: 9.12.2014.
- Anonymous, 2017. Poliüretanların kullanım alanları. www.ema.gen.tr/poliuretanin-kullanim-alanlari/
- Aydın, H., Ekmekçi, İ., 2002. Isı yalıtım malzemesi olarak poliüretan köpüğün fiziksel ve kimyasal özellikleri, üretimi ve incelenmesi. *SAU Fen Bilimleri Enstitüsü Dergisi*, 6(1): 45-50.
- Barikani, M., Mohammadi, M., 2006. Synthesis and characterization of starch-modified polyurethane. *Carbohydrate Polymers*, 68: 773-780.
- Bayülken, Y., Kütükođlu, H. C., 2009. Yalıtım Sektörü Envanter Arařtırması Raporu (İZODER). Mayıs 2009.

http://www.yapi.com.tr/Arastirmalar/yalitim-sektoru-envanter-arastirmasi_393.html. Erişim Tarihi: 06.09.2009.

- Besteu, L., Soyer, N., Bruneau., C. Brault, A., 1965. Wood liquefaction with hydrogen and helium in the presence of iron additives. *The Canadian Journal of Chemical Engineering*, 64:775-780.
- Cinelli, P., Anguillesi, I., Lazzei, A., 2013. Green synthesis of flexible polyurethane foams from liquified lignin. *European Polymer Journal*, 49:1174-1184.
- Ferrigno, T. H., 1967. *Rigid Plastics Foams*. Second Edition. Reinhold Publishing. Corp./Chapman-Reinhold. Newyork, N.Y. s. 146.
- Gang, H., Lee, D., Choi, K.Y., Kim, H.N., Ryu, H., Lee, D.S., Kim, B.G., 2017. Development of high performance polyurethane elastomers using vanillin-based green polyol chain extender originating from lignocellulosic biomass. *ACS Sustainable Chemistry and Engineering*, 5(6): 4582-4588.
- Hakim, A. A. A., Nassar, M., Emam, A., Sultan, M., 2011. Preparation and characterization of rigid polyurethane foam prepared fro sugar-cane bagasse polyol. *Material Chemistry and Physics*, 129: 301-307.
- Hatakeyama H. Hirose S. Hatakeyama, T. Nakamura K., Kabashigawa K., Morohoshi, N., 1992. Biodegradable polyurethane from

- plant components. *J. Macromol. Sci. Part A, Pure Appl. Chem.* 32:743-750.
- Hostettler, F., Barnes, B. K., Mclaughlin R. W., 1963. Polyurethane foams. US 3073788.
- Hsu, O. H.-H., Glasser, W. G., 1979. Polyurethane adhesives and coating from modified lignin. *Wood Sci.*, 9: 97-103.
- Koch, H., Rober, N., 1988. New industrial products from starch. *Stärke*, 40: 121-131.
- Lin, L. Z., Yoshiokam, M., Yao, Y. G., Shiraishi, N., 1994. Liquefaction of wood in the presence of phenol using phosphoric acid as a catalyst and the flow properties of the liquefied wood. *J. Appl. Polym. Sci.*, 52(11): 1629-1636.
- Maldas, D., Shiraishi, N., 1997. Liquefaction of biomass in the presence of phenol and H₂O using alkalies and salts as the catalyst. *Biomass Bioenergy*, 12: 273-279.
- Pan, H., Zheng, Z., Chung, Y. H., 2011. Microwave-assisted liquefaction of wood with polyhydric alcohols and its application in preparation of polyurethane (PU) foams. *J. Wood Prod.*, 70(4): 461-670.
- Savelyev, Yu. V., Veselov, V., Markovskaya, L., Savalyeva, O., Akhranovich, E., Galatenko, N., Robota, L., Travinskaya, T., 2014. Preparation and characterization of new biologically active polyurethane foams. *Materials Science and Engineering C*, 45 (2014): 127-135.

- Trovati, G., Sanches, E.A., Neto, S.C., Mascarenhas, Y.P., Chierice, G.O., 2010. Characterization of polyurethane resins by FTIR, TGA and XRD. *Journal of Applied Polymer Science*, 115: 263-268.
- Vuori, A., Niemela, N., 1988. Liquefaction of kraft lignin II-reaction with a homogenous lewis acid catalyst under mild temperature conditions. *Holzfoschung*, 42: 327.
- Wang, H., Chen, H. Z., 2007. A novel method of utilizing the biomass resource: Rapid liquefaction of wheat straw and preparation of biodegradable polyurethane foam. *Journal of other Chinese Institute of Chemical Engineers*, 38: 95-102.
- Wang, Y., Tian, H., Zhang, L., 2010. Role of starch nanocrystals and cellulose whiskers in synergistic reinforcement of waterborne polyurethane. *Carbohydrate Polymer*, 80: 665-671.
- Wang, M., Zhang, X., Zhang, W., Tian, D., Lu, C., 2013. Thermoplastics of polyurethane composites prepared from mechanochemically activated waste cotton fabric and reclaimed polyurethane foam. *Journal of Applied Polym. Sci.*, 128(6): 3555-3563.
- Wei, F., Enhai, S., Akihiko, F., Hongcai, W., Koichi, N., Katsumi, Y., 2000. Synthesis and characterization of Photoconducting Polyaniline-TiO₂ Nanocomposite. *Bulletin of Chemical Society Japan*, 73(11): 2627-2633.

- Yamada, T., Ona, T., 1999. Rapid liquefaction of lignocellulosic waste by using ethylene carbonate. *Bioresource Technol.*, 70(1): 61.
- Yao, Y., Yoshioka, M., Shiraishi, N., 1993. Combined liquefaction of wood and starch in a polyethylene glycol / glycerin blended solvent. *Mokuzai Gakkaishi*, 39: 930-938.
- Yao, Y., Yoshioka, M., Shiraishi, N., 1996. Water absorbing polyurethane foams from liquefied starch. *J. Appl. Polym. Sci.* 60:1939-1949.
- Yasushi, S., Seizi, N., Shigetake K., 1972. Structural studies on polyurethane fibers.I. Crystal and molecular structures of aliphatic polyurethanes from hexamethylene diisocyanate and some linear glycols. *Polymer Journal*, 3: 113-121.
- Yoshida, H., Morck, R., Kringstad, K. P., Hatakeyama, H., 1987. Kraft lignin in polyurethane I. mechanical properties of polyurethane from a kraft lignin-polyether-triol-polymeric MDI system. *Journal of Applied Polym. Sci.*, 34: 1187-1198.
- Zhang, Y., Leng, Y., Zhu, M., Fan, B., Yan, R., Wu, Q., 2012. Starches modified with polyurethane microparticles: Effects of hydroxyl numbers of polyols in polyurethane. *Carbohydrate Polymers*, 88: 1208, 1213.
- Zou, J., Zhang, F., Huang, J., Chang, P. R., Su, Z., Yu, J., 2011. Effects of starch nanocrystals on structure and properties of

waterborne polyurethane-based composites. *Carbohydrate Polymer*, 85: 824-831.



978-605-7695-24-6



IKSAD
Publishing House